Food Chemistry: X 26 (2025) 102348

Contents lists available at ScienceDirect

Food Chemistry: X

journal homepage: www.sciencedirect.com/journal/food-chemistry-x

Comparative study on the effects of different drying technologies on the structural characteristics and biological activities of polysaccharides from *Idesia polycarpa* maxim cake meal

Qiuqiu Zhang [a], Renshuai Huang [a], Lisha Wang [b], Yonghui Ge [a,c], Honggang Fang [d], Guangjing Chen [a,c,*]

[a] College of Food Science and Engineering, Guiyang University, Guiyang, Guizhou 550005, PR China
[b] Experimental Center, Guizhou Police College, Guiyang, Guizhou 550005, PR China
[c] Engineering Technology Research Center for Processing and Comprehensive Utilization of Idesia polycarpa, National Forestry and Grassland Administration of the People's Republic of China, Guiyang, Guizhou 550005, PR China
[d] Guizhou Lincao Development Co., Ltd, Guiyang, Guizhou 550001, PR China

ARTICLE INFO

Keywords:
Idesia polycarpa maxim polysaccharides
Microwave vacuum drying
Structure characteristic
Antioxidant activity
Anti-glycation activity
Hypoglycemic activity

ABSTRACT

To extract oil, the fruits of *Idesia polycarpa* Maxim (IPM) must first undergo a drying process. This study aimed to investigate how different industrial drying techniques—microwave vacuum drying (MVD), microwave drying, infrared drying, and hot air drying—affect the structural characteristics and bioactivities of IPM cake meal polysaccharides (IPMPs). The results revealed significant differences in the structure and composition of the four IPMPs. MVD-IPMP, dried using MVD, exhibited a lower molecular weight (346.26 kDa), higher uronic acid content (30.74 %), and a distinct triple-helix structure. These structural features contributed to its enhanced antioxidant activity, α-glucosidase inhibition, and prevention of glycation. IPMPs induced secondary conformational changes in α-glucosidase, leading to decreased enzyme activity. Additionally, IPMPs caused static quenching of the enzyme's intrinsic fluorescence, suggesting a specific interaction mechanism, with MVD-IPMP demonstrating the highest binding affinity. These findings suggest that MVD is an effective technique for the large-scale production of high-quality IPMPs.

1. Introduction

Idesia polycarpa Maxim (IPM) is the sole species in the genus *Idesia*, part of the Salicaceae family. This woody perennial oil plant is extensively found across East Asia, encompassing China, Japan, and Korea (Li et al., 2019; Li et al., 2020). In recent years, IPM has gained increasing attention due to its excellent adaptability, attractive appearance, high yield, and prolonged fruiting period. These traits contribute to its superior oil content and quality compared to other common woody oil crops. IPM oil is regarded as a promising solution to the rising demand for edible and industrial oils, as well as energy and other resources (Luo et al., 2025; Wen et al., 2022). IPM oil has been used as an edible oil in China for over a century. It is abundant in polyunsaturated fatty acids, especially linoleic acid, and includes important bioactive compounds like β-sitosterol, α-tocopherol, and β-tocopherol (Xiang et al., 2023). Research has shown that IPM not only yields large quantities of oil from its fruit but also contains oil in both the seeds and peel. As the fruit matures, the oil content in the peel increases, making the entire fruit valuable for industrial oil extraction (Hou et al., 2018; Zhou et al., 2022). However, processing IPM fruits for oil generates large quantities of byproducts, commonly known as cake meal. If not managed properly, these byproducts can lead to environmental problems and resource waste, hindering the growth of the IPM industry. Therefore, developing effective methods for utilizing IPM cake meal is essential. Such utilization would enhance its economic value, reduce resource waste, and alleviate environmental pressures caused by untreated byproducts. Early studies have identified several beneficial components in IPM cake meal, including peptides, proteins, and polysaccharides. For example, Dou et al. (2024) isolated antioxidant peptides (CIPs-I-F2) from IPM cake meal, while Yang et al. (2023) utilized proteins from the meal to

* Corresponding author at: College of Food Science and Engineering, Guiyang University, 103 Jianlongdong Road, Nanming District, Guiyang, Guizhou 550005, PR China.
E-mail addresses: gyugjchen@gyu.edu.cn, gjchen1989@126.com (G. Chen).

https://doi.org/10.1016/j.fochx.2025.102348
Received 18 January 2025; Received in revised form 27 February 2025; Accepted 5 March 2025
Available online 7 March 2025

develop bioactive food packaging materials that extend the shelf life of sweet cherries. Our earlier study utilized ultrasound-assisted three-phase extraction to isolate oils, proteins, and polysaccharides from IPM cake meal, highlighting its high polysaccharide (10.02 %) and protein (5.03 %) content (Shi et al., 2024). Given its high content of proteins and polysaccharides, the secondary use of IPM cake meal aligns with the principles of a circular economy. This approach minimizes resource waste, maximizes the value derived from IPM, and supports sustainable development while reducing environmental impact.

Polysaccharides, natural polymers found in plants, microorganisms, and animals, are widely utilized in the pharmaceutical and food industries due to their unique biological properties and superior safety profiles (Tian et al., 2022; Yu et al., 2018). These macromolecules have garnered significant attention due to their diverse biological activities, including anti-inflammatory (Jin et al., 2021), antioxidant (Chen et al., 2022), immunomodulatory (Mohammed et al., 2021), hypoglycemic (Xiong et al., 2022), and gut microbiota-regulating effects (Ye et al., 2023). In industrial processes, oil seeds are dried and dehydrated prior to oil extraction using methods such as hot air drying (HD), infrared drying (IRD), microwave drying (MD), and freeze drying (FD) (Menon et al., 2020). Each method offers distinct advantages and challenges in terms of cost, time efficiency, and operational complexity. Research shows that drying substantially influences the structural properties and bioactivities of polysaccharides, altering molecular weight, monosaccharide composition, branching patterns, chain conformation, antioxidant capacity, digestive enzyme inhibition, and emulsifying properties (An et al., 2022; Yi et al., 2020). HD is prevalent in the food industry because it is simple and cost-effective. This method involves circulating heated air over the material to facilitate moisture evaporation. Research indicates that HD notably elevates the molecular weight of polysaccharides in okra (*Abelmoschus esculentus*) relative to alternative drying techniques (Yuan, He, Xiang, Huang, et al., 2020). In contrast, IRD uses infrared radiation to uniformly heat the material, thereby enhancing drying efficiency (Zartha Sossa et al., 2021). However, IRD may alter the steric conformation of polysaccharides, potentially changing their functional properties (Yan et al., 2019). MD generates heat through molecular friction, enabling rapid drying with minimal oxygen exposure. However, the higher temperatures associated with MD can cause slight thermal aggregation of polysaccharides (Wu et al., 2022). FD which removes moisture by sublimation of frozen water under low pressure, preserves a loose, porous structure with minimal aggregation, thereby improving stability (Chen et al., 2020). However, FD is hindered by long drying times and high energy consumption. Emerging technologies, such as microwave-assisted vacuum drying (MVD), offer advantages over traditional methods. MVD prevents structural changes caused by oxygen exposure, ensures uniform heat distribution, and provides precise control over drying parameters (Kubbutat et al., 2021; Liu, Li, et al., 2020). Excessively high temperatures and prolonged drying times can result in the thermal degradation of natural polysaccharides during the drying process. This degradation can cause structural changes that negatively impact the long-term stability and storage quality of the polysaccharides (Guo, Liu, et al., 2023). Therefore, it is essential to select appropriate drying methods based on the type of raw material and the specific polysaccharide involved. Given the varying effects of different drying methods on polysaccharide properties, selecting an appropriate method is critical for preserving both their physicochemical integrity and biological activities. While the effects of drying on the structure and biological activities of plant-derived polysaccharides are well documented (Guo, Yin, et al., 2023; Yi et al., 2020), the specific impacts of various drying methods on polysaccharides derived from IPM cake meal remain unexplored.

Diabetes is a chronic metabolic disorder marked by physiological issues such as low blood sugar, insufficient insulin production and release, and excessive glucagon secretion (Yang et al., 2024; Yang, Luo, Wei, & Kan, 2022). Polysaccharides have been shown to combat diabetes through multiple mechanisms in both laboratory settings and living organisms (Dong et al., 2023; Ji et al., 2023; Xue et al., 2023). Two key enzymes involved in glucose metabolism are pancreatic α-amylase and intestinal α-glucosidase. Inhibiting these enzymes slows the breakdown of starches into glucose, thus reducing postprandial blood sugar spikes (Dou et al., 2019; Meng et al., 2019). Targeting α-amylase and α-glucosidase represents a promising strategy for managing blood glucose levels in diabetic individuals. Chronic hyperglycemia in diabetes hastens the non-enzymatic glycation of proteins, resulting in the formation of advanced glycation end products (AGEs) (Zhang et al., 2022). During this process, reducing sugars interact with protein amino groups, leading to the irreversible creation of AGEs (Zeng et al., 2016). AGEs interact with vascular endothelial cell receptors, triggering the activation of RAGE. This activation triggers cellular pathways and oxidative stress, contributing to diabetic complications, particularly those affecting blood vessels (van Dongen et al., 2021). Consequently, compounds that inhibit AGEs formation hold potential as therapeutic agents to prevent diabetes-related complications. Free radicals and reactive oxygen species (ROS) significantly contribute to diabetes development (Rotariu et al., 2022). ROS are generated via glucose oxidation, protein glycation, and lipid peroxidation (Meng et al., 2019). A major marker of lipid peroxidation is malondialdehyde (MDA), a toxic compound indicative of oxidative damage. Preventing MDA formation could help alleviate oxidative stress associated with diabetes (Dong et al., 2023; Yang et al., 2024). Antioxidants with notable blood sugar-lowering and antiglycation effects may provide therapeutic benefits for diabetes management and its complications. Several studies have demonstrated that different drying methods can alter the physical and structural properties of polysaccharides, which in turn can affect their biological activities (Shiyu et al., 2024; Tang et al., 2023; Yang, Luo, Sang, & Kan, 2022). We hypothesize that the drying techniques applied to IPM cake meal may similarly influence the properties of its polysaccharides. However, there is currently a lack of research on how various drying methods affect polysaccharides extracted from IPM cake meal. Exploring this gap may lead to innovative uses of IPM cake meal in food science and health, especially in creating functional foods and natural diabetes treatments.

Therefore, this study examined the effects of four drying methods—microwave drying (MD), microwave vacuum drying (MVD), infrared drying (IRD), and hot air drying (HD)—on the polysaccharides extracted from IPM cake meal (IPMPs). The chemical composition of the polysaccharides was analyzed, focusing on parameters such as neutral sugars, uronic acids, protein content, molecular weight, and sugar composition. Structural characteristics were examined using triple-helix conformation analysis, Fourier-transform infrared (FT-IR) spectroscopy, scanning electron microscopy (SEM), and X-ray diffraction (XRD). In addition to chemical and structural analyses, the biological properties of IPMPs were evaluated, specifically its ability to inhibit linoleic acid oxidation, prevent the formation of AGEs, and block α-glucosidase activity through laboratory assays. The results of this study will provide valuable insights into how different drying methods affect the structure and biological properties of IPMPs. These findings will aid in identifying optimal drying techniques for producing IPMPs with antioxidant, antiglycation, and hypoglycemic effects, thus facilitating their application in the development of functional foods and natural treatments for diabetes management.

The study of polysaccharides derived from IPM cake meal not only explores their potential applications in the food and pharmaceutical industries but also provides a sustainable solution to the environmental challenges associated with their disposal. This contributes to enhancing the overall sustainability of the IPM processing industry.

2. Materials and methods

2.1. Reagent and chemicals

On November 11, 2023, fresh IPM fruits were harvested from Xinhua

Feng Agricultural Development Co., Ltd., located in Renhuai City, Guizhou Province (27°59′5.23″N, 106°18′38.07″E). The fruits, all from the same batch, were stored at temperatures ranging from 4 °C to 8 °C prior to drying. D-Galacturonic acid monohydrate (SG8830) and Bovine Serum Albumin (BSA, A8020) was purchased from Solarbio Technology Co., Ltd. (Beijing, China). A range of monosaccharide standards, including D-mannose (Man, C17D9H77586), L-rhamnose (Rha, H10S9Z69863), D-galactose (Gal, E1927035), D-glucose (Glc, Q18F10N80946), L-arabinose (Ara, S15A10G85850), D-xylose (Xyl, A22S6X3606), L-fucose (Fuc, X29D7Y27768), D-galacturonic acid (GalA, K02A9B66077), and D-glucuronic acid (GlcA, K14M10S82777) were obtained from TOKYO Chemical Industry Co., Ltd. (Tokyo, Japan). The pullulan polysaccharide calibration kit was supplied by Agilent Co., (USA). Linoleic acid (L812257) and aminoguanidine hydrochloride (AG, H905587) were provided by Macklin Biochemical Co., Ltd. (Shanghai, China). Additionally, α-glucosidase (S10050) was acquired from YuanYe Biotech Co., Ltd. (Shanghai, China), while *p*-nitrobenzene α-D-pyran glucoside (*p*NPG, N100372) was obtained from Aladdin Biochemical Technology Co., Ltd. (Shanghai, China). All other chemicals used were of analytical or chromatographic grade and were procured locally.

2.2. Drying procedure and cake meal preparation

The freshly harvested IPM fruits, each group weighing 4.0 kg, were divided into four groups and subjected to distinct drying methods: microwave vacuum drying (MVD), microwave drying (MD), infrared drying (IRD), and hot air drying (HD). To minimize browning, fresh IPM fruits were dried under optimal conditions derived from preliminary experiments. As shown in Fig. 1, in the MVD group, fruits were dried using a commercial microwave vacuum dryer (Model WBZ-10 PLC, Xinqi Microwave Industry Co., Ltd., Guiyang, China) at a vacuum pressure of 0.08 MPa for 55 min. The drying process involved an automated cycle of 35 min at 2000 W, 10 min at 1000 W, 5 min at 500 W, and 5 min at 0 W. In the MD group, fruits were dried using a 1500 W microwave vacuum drying oven (Model WBZ-10 PLC, Xinqi Microwave Industry Co., Ltd., Guiyang, China) for 60 min with the vacuum pump

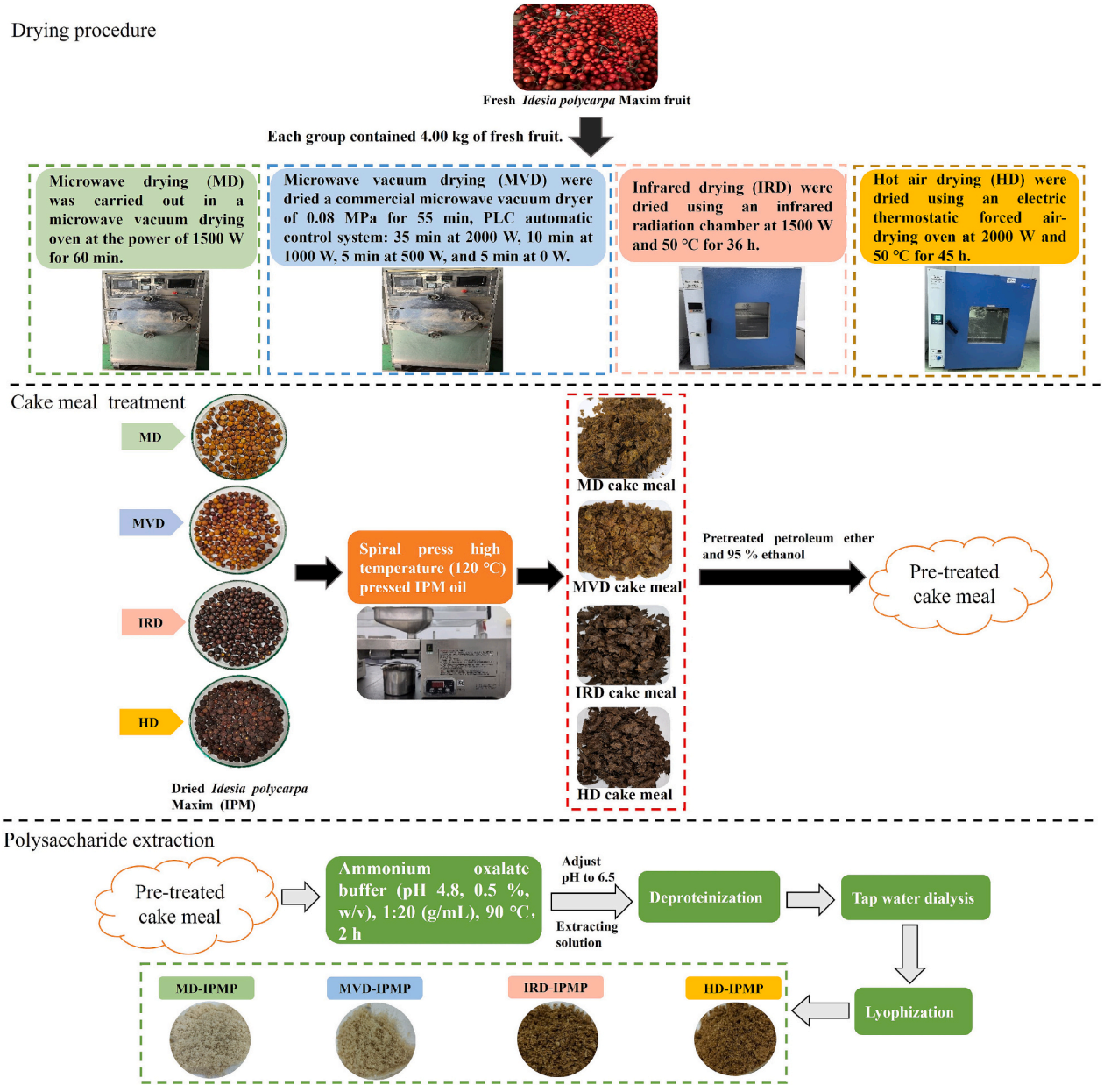

Fig. 1. Schematic of polysaccharides extraction from *Idesia polycarpa* Maxim cake meal.

deactivated. In the IRD group, fruits were dried using an infrared radiation chamber (Model DHG-9202-3, Henglong Instrument Co., Ltd., Changzhou, China) at 1500 W and 50 °C for 36 h. In the HD group, the drying process was conducted in an electric thermostatic forced air-drying oven (Model DHG-9240 A, Qixin Scientific Instruments Co., Ltd., Shanghai, China) at a power setting of 2000 W and a temperature of 50 °C for 45 h. The drying was considered complete when the moisture content of the IPM fruit fell below 6 % (wet basis). The dried fruits were promptly processed with a spiral oil press (Model CZR081, Dehaiwei Industrial Equipment Co., Ltd., Guangzhou, China) for oil extraction. The cake meal was processed using a multifunction mill (Model BJ-800 A, Deqing Fengjie Electric Appliance Co., Ltd., Guangzhou, China) and passed through a 40-mesh screen to achieve a consistent particle size for further experiments.

2.3. Extraction of polysaccharides from IPM cake meal

The cake meal underwent a 24 h petroleum ether soak, with solvent replacement every 6 h, to eliminate residual oil, monosaccharides, and pigments. Subsequently, it was treated with 95 % ethanol for another 24 h, refreshing the ethanol every 6 h. The polysaccharide extraction and separation process are illustrated in Fig. 1. Polysaccharides were extracted via the chelator method by mixing cake meal with an ammonium oxalate buffer (0.5 % *w/v*, pH 4.8) at a solid-to-liquid ratio of 1:20 and heating at 90 °C for 2 h (Babbar et al., 2016). The pH was adjusted to 6.5 with 1 M NaOH following extraction. The mixture was centrifuged at 4000 rpm for 10 min, and the supernatant, containing the polysaccharides, was separated. Proteins were removed by treating the supernatant six times with Sevag reagent, a mixture of chloroform and *n*-butanol in a 4:1 ratio (Sevag et al., 1938). The purified extract was concentrated to one-quarter of its initial volume using a rotary evaporator at 54 °C under reduced pressure, then dialyzed against tap water (MWCO 8000–14,000 Da) for 48 h. The retained material was subsequently collected, concentrated, and freeze-dried under vacuum to isolate the polysaccharides. Polysaccharides derived from IPM cake meal dried by different methods—MD, MVD, IRD, and HD—were designated as MD-IPMP, MVD-IPMP, IRD-IPMP, and HD-IPMP, respectively. The yield (%) of IPMP was determined using the equation:

$$\text{IPMP yield } (\%, w/w) = \frac{\textit{Weight of dried IPMP } (g)}{\textit{Initial weight of pretreated IPM cake meal powder } (g)} \times 100 \quad (1)$$

2.4. The chemical compositions analysis of IPMPs

2.4.1. The neutral sugar, uronic acid and protein content of IPMPs

The contents of neutral sugars, uronic acids, and proteins in IPMPs were determined using the phenol-sulfuric acid method for neutral sugars (Dubois et al., 1956), the *m*-hydroxyphenyl method for uronic acids (Blumenkr & Asboehan, 1973), and the Coomassie brilliant blue method for proteins (Zor & Seliger, 1996), respectively.

2.4.2. Monosaccharide composition analysis

The monosaccharide composition of IPMPs was analyzed using high-performance anion-exchange chromatography (HPAEC) on a Thermo Dionex ICS-6000 system (Thermo Scientific, Waltham, MA, USA), following previous method (Wan et al., 2025). A 6 mg IPMP sample was combined with 3 mL of 3 M trifluoroacetic acid (TFA) in an amber vial, which was then sealed using an alcohol burner. Hydrolysis was carried out at 121 °C for 3 h. After cooling, the solution was concentrated under reduced pressure and stirred to remove the TFA. The residue was dissolved in distilled water and the volume was adjusted to 50 mL. Prior to analysis, the sample was filtered through a 0.22 μm membrane. Chromatographic separation was performed on a Dionex CarboPac PA20 column (3 mm × 150 mm) with a CarboPac PA20 guard column (3 mm × 30 mm) and electrochemical detection. The column temperature was maintained at 30 °C, the flow rate was set to 0.25 mL/min, and 25 μL of the sample was injected. The mobile phases consisted of ultrapure water (A), 20 mM NaOH (B), 500 mM sodium acetate (C), and 100 mM NaOH (D), and the gradient elution was as follows: 0–20 min: 90.5 % A, 9.5 % B; 20.01–36 min: 70 % A, 10 % B, 20 % C; 36.05–50 min: 50 % A, 50 % D. To ensure accurate identification and quantification, a mixture of nine standard monosaccharides (at concentrations of 1, 2.5, 5, and 10 ppm) was prepared and analyzed under identical conditions. The standard curves and HPAEC chromatograms of the monosaccharide standards are presented in Table S1 and Fig. S1, respectively. The monosaccharide composition and molar percentages were determined by comparing retention times and peak areas with those of the standards.

2.4.3. Molecular weight (mw) distribution analysis

The *Mw* distribution of IPMPs was analyzed via high-performance gel permeation chromatography (HPGPC, Agilent 1260, Agilent Technologies, Santa Clara, CA, USA) with a refractive index detector (1260 RID, Agilent Technologies). A standard curve ($y = -0.4397\times + 11.6923$, $R^2 = 0.9976$) was established using molecular weight markers ranging from 6.3 to 334 kDa (6.3, 9.8, 22, 49.7, 107, 216, 334 and 739 kDa). The corresponding HPGPC chromatograms for the molecular weight standards are presented in Fig. S2. 2 mL of IPMPs solution (5 mg/mL) was filtered using a 0.45 μm membrane and analyzed using a TSK-Gel GMPWXL column (7.8 mm × 300 mm, Tosoh Bioscience, Tokyo, Japan). The analysis was conducted using a mobile phase of 0.1 M $NaNO_3$, with a 25 μL injection volume, a column temperature set to 30 °C, and a flow rate of 0.5 mL/min. Under these conditions, the molecular weight distribution of the IPMP samples was effectively analyzed, with elution completed within 36 min.

2.5. Characterizations of IPMPs

2.5.1. FT-IR spectroscope analysis

Infrared spectra of IPMPs were obtained using the KBr pellet method on a FT-IR spectrometer (Spectrum Two, PerkinElmer Co., Waltham, MA, USA) (Jia et al., 2020). For sample preparation, 2 mg of IPMPs and 200 mg of potassium bromide were accurately weighed, ground in an agate mortar, and compressed into translucent pellets. A pure KBr pellet was used as the reference. Spectral data were acquired between 400 and 4000 cm^{-1} with a 4 cm^{-1} resolution.

2.5.2. Congo red test

The Congo Red method, as described by Shi et al. (2024), was used to assess the triple-helix structure of IPMPs. A 2 mL solution of IPMPs (2 mg/mL) was mixed with 2 mL of Congo red solution (80 μM). The mixture was titrated incrementally with 1.0 M NaOH (0–4 mL) to achieve a final concentration range of 0–0.50 M NaOH. The solution was

incubated at room temperature for 15 min, and its absorbance was recorded between 400 and 600 nm using a multifunctional microplate reader (Multiskan SkyHigh-A51119600C, Thermo Scientific, Waltham, MA, USA). A control was prepared using deionized water under identical conditions.

2.5.3. Thermal property analysis

The thermal stability of the IPMPs was evaluated using a differential scanning calorimeter (DSC-4000, PerkinElmer Co., Waltham, MA, USA). Approximately 5 mg of IPMPs was sealed in a pure aluminum crucible, while an empty crucible was used as the reference. The sample was heated from 50 °C to 400 °C at a rate of 10 °C/min under a nitrogen flow of 20 mL/min to determine its denaturation temperature.

2.5.4. XRD analysis

The crystalline structure of IPMPs was evaluated using a D8 Advance diffractometer (Bruker, Bremen, Germany) operating at 40 mA. XRD patterns were collected over the range of 5°–80° at a scanning speed of 10°/min.

2.5.5. SEM analysis

The structural features of IPMPs were observed using a SIGMA 300 scanning electron microscope (ZEISS, Oberkochen, Germany). For each analysis, 20 mg of polysaccharides were placed onto SEM aluminum stubs using double-sided adhesive tape. To enhance imaging quality, the samples were coated with a thin gold-palladium layer using a sputter coater. High-resolution images were acquired at magnifications of 100×, 5000×, and 10,000×, using an acceleration voltage of 3.0 kV.

2.6. Non-enzymatic glycation inhibition activity

2.6.1. Establishment of the BSA-fructose reaction system

The in vitro anti-glycation assay was conducted following a modified method (Zhou et al., 2023). Sample solutions were prepared in phosphate buffer (0.2 M, pH 7.4). The reaction system was set up by mixing 5 mL of BSA solution (10 mg/mL) with 2.5 mL of polysaccharide solution (1, 2, 3, or 4 mg/mL), followed by the addition of 5 mL of fructose solution (500 mM). The mixture was incubated at 50 °C for 48 h. Control experiments included a blank control, in which the polysaccharide solution was replaced with buffer, and a positive control, in which AG replaced the polysaccharide solution. The resulting mixtures were used in subsequent analyses.

2.6.2. Determination of fructosamine level

Fructosamine levels were determined by their ability to reduce nitroblue tetrazolium (NBT) to the tetrazinolyl radical (NBT^+), forming a colored formazan dye with strong absorbance at 530 nm. The NBT reduction method, as described by Zeng et al. (2019), was applied to measure fructosamine in the BSA-Fructose-IPMP system. In the assay, the reaction mixture (40 μL) was combined with of Milli-Q water (320 μL) and NBT solution (1.6 mL, 0.3 mM in 100 mM sodium carbonate buffer, pH 10.35). After incubating at 25 °C for 15 min, the mixture was measured the absorbance at 530 nm. Blank and positive controls were included for comparison. The inhibition rate of fructosamine was calculated using the following formula:

$$\textit{Inhibition rate}\ (\%) = \left(\frac{A_0 - A}{A_0}\right) \times 100 \tag{2}$$

where A_0 is the absorbance of the BSA-Fructose system without polysaccharides, and A indicates is the absorbance with polysaccharides.

2.6.3. Determination of α-dicarbonyl compounds

The levels of α-dicarbonyl compounds were quantified using the Girard-T reagent and spectrophotometry (Dou et al., 2021). In this test, the reaction mixture (0.4 mL) was combined with Girard-T stock solution (0.2 mL, 500 mM) and sodium formate solution (3.4 mL, 500 mM, pH 2.9). The mixture was incubated at 37 °C for 60 min, after which the absorbance of both the blank control and positive control was measured at 290 nm. The inhibition rate of α-dicarbonyl compounds was estimated using the formula previously described (Eq.(2)).

2.6.4. Determination of the fluorescent AGEs

The formation of fluorescent AGEs was assessed by combining 60 μL of the reaction solution with 2 mL of phosphate-buffered saline (PBS, 0.2 M, pH 7.4). The fluorescence intensity of the mixture was tested using a fluorescence spectrophotometer, with an excitation wavelength of 370 nm and an emission wavelength of 450 nm (Dou et al., 2021). The inhibition rate of fluorescent AGEs was calculated using the following formula:

$$\textit{Inhibition rate}\ (\%) = \left(\frac{F_0 - F}{F_0}\right) \times 100 \tag{3}$$

where F_0 is the fluorescence intensity of the BSA-Fructose system without polysaccharides, and F is the fluorescence intensity with polysaccharides.

2.7. Linoleic acid peroxidation inhibition assay

The ability of IPMPs to prevent linoleic acid peroxidation was evaluated by measuring the MDA levels in a linoleic acid system, following a previously established procedure (Chaouch et al., 2015). To prepare the reaction mixture, 4.1 mL of linoleic acid-ethanol solution (2.5 %, *v/v*), 10 mL of phosphate buffer (0.2 M, pH 7.4), 4.9 mL of distilled water, and 1 mL of 4 mM $FeSO_4{\cdot}7H_2O$ were combined. IPMP solutions (0.125–5 mg/mL) were then added to the mixture, which was thoroughly mixed and incubated at 40 °C for 24 h. Following incubation, 1 mL of the reaction mixture was taken, and 1 mL of 25 % trichloroacetic acid (TCA) and 2 mL of 0.67 % thiobarbituric acid (TBA) were added. The mixture was heated in boiling water for 15 min, allowed to cool, and then 4 mL of *n*-butanol was added. Absorbance was measured at 532 nm, with deionized water used as the blank and V_C serving as the positive control. The inhibition rate of linoleic acid peroxidation was calculated as follows:

$$\textit{Inhibition rate}\ (\%) = \left(1 - \frac{A_S}{A_0}\right) \times 100 \tag{4}$$

where: A_S represents the absorbance of the sample containing IPMP, and A_0 represents the absorbance when deionized water is used instead of IPMPs.

2.8. Hypoglycemic activities

2.8.1. α-Glucosidase inhibitory activity analysis

The ability of IPMPs to inhibit α-glucosidase was assessed using a method adapted from Zheng et al. (2022). All solutions were prepared in phosphate buffer (0.1 M, pH 6.9). For the assay, 100 μL of IPMPs at varying concentrations (0.5, 1, 2, 4, 6 mg/mL) was mixed with 100 μL of α-glucosidase solution (0.5 U/mL) and incubated at 37 °C for 10 min. The reaction was initiated by adding 100 μL of *p*NPG solution (5 mM) and incubated for an additional 20 min. The reaction was then terminated by adding 1 mL of 1 M sodium carbonate solution, and absorbance was measured at 405 nm. The buffer served as the blank control, and acarbose was used as the positive control. The inhibition rate of α-glucosidase was calculated using the following formula:

$$\alpha - \textit{Glucosidase inhibition rate}\ (\%) = \left(1 - \frac{A_S - A_B}{A_C}\right) \times 100 \tag{5}$$

where A_S represents the absorbance of the mixture containing IPMPs, enzyme, and *p*NPG. A_B represents the absorbance when buffer is used

instead of the enzyme. A_C represents the absorbance of the buffer solution, which serves as a replacement for the sample solution.

2.8.2. Kinetic property analysis

To study the kinetic properties of IPMP's inhibition of α-glucosidase, the concentrations of IPMP (0, 1, 3, and 6 mg/mL) and *p*NPG (1, 2, 3, and 4 mM) were varied. Lineweaver-Burk double reciprocal plots were employed to determine the inhibition type by analyzing the intersection points of the lines. This approach also enabled the comparison of kinetic parameters related to α-glucosidase inhibition at different IPMP concentrations. The Michaelis constant (K_m) and maximum reaction velocity (V_{max}) were determined by plotting $1/v$ against $1/[S]$ using the Lineweaver-Burk equation, based on parameters from the Michaelis-Menten equation. This provided insights into the enzymatic reaction. Mixed-type inhibition was identified, which was further analyzed using Eq.(6) to ascertain the dissociation constants K_i and K_{is} for enzyme-inhibitor and inhibitor–enzyme–substrate interactions of IPMPs. Secondary plots based on Eq.(7) and (8) were generated to refine the understanding of the inhibition mechanism (Wang et al., 2020).

$$\frac{1}{v}=\frac{K_m}{V_{\max}}\left(1+\frac{[I]}{K_i}\right)\frac{1}{[S]}+\frac{1}{V_{\max}}\left(1+\frac{[I]}{K_{is}}\right) \tag{6}$$

$$\text{Slope}=\frac{K_m}{V_{max}}+\frac{K_m[I]}{V_{max}K_i} \tag{7}$$

$$\text{Y-intercept}=\frac{1}{V_{max}}+\frac{[I]}{K_{is}V_{max}} \tag{8}$$

where v was the enzyme reaction rate in the absence and presence of IPMPs. $[I]$ and $[S]$ are the concentrations of inhibitor and substrate, respectively. K_i and K_{is} stand for enzyme–inhibitor dissociation constant and inhibitor–enzyme–substrate dissociation constant, respectively.

2.8.3. Fluorescence spectra analysis

The interaction between IPMPs and α-glucosidase was examined by mixing 2 mL of IPMPs (0.5–6 mg/mL) with 2 mL of 0.75 U/mL α-glucosidase solution. The mixtures were incubated at 37 °C for 10 min, and the fluorescence intensity of the α-glucosidase-IPMP complex was tested using a fluorescence spectrometer with an excitation slit of 5 nm, an emission slit of 5 nm, an excitation wavelength of 280 nm, an emission wavelength range of 300–500 nm, and a scanning rate of 1200 nm/min. To explore the quenching mechanism between IPMPs and α-glucosidase, fluorescence quenching data were analyzed using the Stern-Volmer equation (Eq.(9)) (Zhao et al., 2021):

$$F_0/F=1+K_q\tau_o[Q]=1+K_{sv}[Q] \tag{9}$$

where F_0 represents the enzyme's fluorescence intensity without IPMPs, while F denotes the intensity post-IPMPs addition. $[Q]$ indicates the IPMPs concentration, K_{SV} is the Stern-Volmer quenching constant, K_q is the dynamic quenching rate constant, and τ_0 is the fluorophore's lifetime without the quencher (10^{-8} s).

The fluorescence quenching mechanism was analyzed to calculate the binding constant (K_a) and the number of binding sites (n) between IPMPs and α-glucosidase using the binding constant formula (Eq.(10)) (Zhao et al., 2021):

$$log\frac{F_0-F}{F}=logK_a+nlog[Q] \tag{10}$$

2.8.4. Conformational change assay

To assess potential changes in the secondary structure of α-glucosidase induced by IPMPs, FT-IR spectroscopy was conducted following a previously established method (Tang et al., 2019). A solution containing 100 μL of 5 mg/mL IPMPs and 100 μL of 0.5 U/mL α-glucosidase was incubated at 37 °C for 30 min. The mixture was then applied to a KBr sheet, and the FT-IR spectrum was recorded in the 1500–1800 cm^{-1} wavenumber range. The relative content of the enzyme's secondary structure was analyzed using PeakFit V4 software. Ultraviolet (UV) absorption spectra of α-glucosidase, both in the presence and absence of IPMPs, were obtained using a multifunctional enzyme marker (Zhao et al., 2023). α-Glucosidase was prepared at 0.5 U/mL, and IPMP solutions were evaluated at 0.5, 1.0, 2.0, 4.0, and 6.0 mg/mL. The absorption spectra in the 200–400 nm range were measured after incubating equal volumes of IPMP and α-glucosidase at 37 °C for 30 min to assess IPMP's structural impact on the enzyme.

2.9. Statistical analysis

All experimental data are presented as the mean ± standard deviation (SD) from at least three independent replicates. Statistical analyses, including graphical representation and ANOVA, were conducted using Origin 2019 (Origin Lab Corp., USA) and SPSS 22.0 (SPSS Inc., USA). The Least Significant Difference (LSD) test and Duncan's Multiple Range Test were employed for multiple comparisons to identify statistically significant groups ($p < 0.05$).

Table 1
Extraction yield, chemical composition, monosaccharide composition, molecular weight distribution, and DSC curve parameters of polysaccharides from IPM cake meal dried by different methods.

	MD-IPMP	MVD-IPMP	IRD-IPMP	HD-IPMP
Yield (%)	9.35 ± 0.49^{b}	10.35 ± 0.36^{a}	8.74 ± 0.89^{bc}	8.15 ± 1.03^{c}
Chemical composition (%, *w/w*)				
Neutral sugar	56.93 ± 0.83^{c}	63.46 ± 0.63^{a}	59.66 ± 1.22^{b}	59.26 ± 0.90^{b}
Uronic acid	25.75 ± 0.64^{b}	30.74 ± 1.85^{a}	24.05 ± 0.76^{c}	23.87 ± 0.59^{c}
Protein	4.76 ± 0.43^{ab}	5.09 ± 0.65^{a}	4.06 ± 0.28^{b}	3.72 ± 0.05^{c}
Monosaccharide composition (molar ratio, %)				
Fuc	0.04 ± 0.03^{c}	0.27 ± 0.06^{b}	1.06 ± 0.75^{a}	0.34 ± 0.16^{b}
Rha	8.89 ± 0.99^{b}	11.22 ± 1.14^{a}	9.93 ± 0.16^{ab}	9.27 ± 0.42^{b}
Ara	4.80 ± 2.73^{c}	12.03 ± 0.55^{a}	8.51 ± 0.70^{b}	9.21 ± 0.84^{b}
Gal	6.74 ± 2.45^{b}	12.18 ± 0.11^{a}	11.44 ± 0.59^{a}	11.29 ± 0.25^{a}
Glc	51.27 ± 1.48^{a}	24.57 ± 1.30^{c}	33.84 ± 0.91^{b}	32.20 ± 0.62^{b}
Xyl	1.63 ± 0.33^{b}	3.20 ± 0.30^{a}	2.59 ± 0.59^{a}	2.85 ± 0.15^{a}
Man	0.79 ± 0.62^{c}	3.04 ± 0.29^{a}	2.46 ± 0.87^{b}	3.49 ± 0.53^{a}
GalA	25.06 ± 1.59^{c}	32.34 ± 1.00^{a}	29.01 ± 1.35^{b}	30.23 ± 1.07^{ab}
GlcA	0.79 ± 0.03^{b}	1.14 ± 0.13^{a}	1.16 ± 0.05^{a}	1.12 ± 0.12^{a}
Molecular weight distribution				
Mw (kDa)	370.67 ± 9.99^{b}	346.26 ± 10.83^{c}	396.27 ± 5.63^{a}	337.87 ± 6.72^{c}
Mn (kDa)	98.32 ± 2.24^{d}	88.67 ± 7.78^{c}	122.66 ± 5.32^{a}	108.09 ± 1.74^{b}
Mw/Mn	3.77 ± 0.14^{a}	3.92 ± 0.31^{a}	3.23 ± 0.10^{b}	3.13 ± 0.03^{b}
DSC curve parameters				
Tm (°C)	139.80 ± 1.41^{b}	146.24 ± 8.94^{a}	137.44 ± 2.83^{b}	139.67 ± 9.55^{b}
Δ*Hm* (J/g)	99.02 ± 10.89^{c}	191.27 ± 5.61^{a}	174.57 ± 40.48^{b}	197.27 ± 18.85^{a}
To (°C)	296.80 ± 4.34^{a}	243.89 ± 2.40^{b}	240.03 ± 0.77^{b}	239.78 ± 2.18^{b}
Tg (°C)	317.61 ± 1.99^{a}	256.09 ± 5.53^{b}	255.66 ± 6.12^{b}	254.36 ± 2.31^{b}
Δ*Hg* (J/g)	5.22 ± 1.16^{c}	9.05 ± 0.67^{b}	22.17 ± 12.81^{a}	11.76 ± 1.46^{b}

Data are expressed as mean ± standard deviation ($n = 3$). Different lowercase letters within the same row indicate significant differences among samples ($p < 0.05$).

3. Results and discussion

3.1. The yield and chemical composition of different IPMPs

3.1.1. The yield of IPMPs

The extraction yields of IPMPs processed using MD, MVD, HD, and IRD are summarized in Table 1. The yields for MD-IPMP, MVD-IPMP, IRD-IPMP, and HD-IPMP were 9.35 %, 10.35 %, 8.74 %, and 8.15 %, respectively. MVD-IPMP achieved the highest yield, significantly outperforming the other methods ($p < 0.05$), highlighting the impact of drying techniques on polysaccharide extraction. Both MD and MVD treatments were more efficient in extracting polysaccharides than HD and IRD. The superior yield in MVD can be attributed to the high vapor pressure generated by microwaves, which disrupt cell wall integrity, enhancing polysaccharide release (Gavahian et al., 2021). Additionally, the vacuum expansion during MVD promotes better penetration of the extraction solvent into plant tissues, further improving extraction efficiency (Dong et al., 2021; Guo, Yin, Wu, Chen and Ye, 2023). These combined effects likely explain the highest polysaccharide yield observed in MVD-treated samples. In contrast, HD resulted in the lowest yield, likely due to the "case hardening" effect, where the material's surface hardens during hot air drying, limiting extraction efficiency (An et al., 2022). Despite these variations, all drying methods yielded satisfactory results, confirming polysaccharide extraction as an effective approach for utilizing IPM cake meal.

3.1.2. The neutral sugar, uronic acid and protein content of IPMPs

Regarding the neutral sugar content, MVD-IPMP had the highest proportion (63.46 %), followed by IRD-IPMP (59.66 %), HD-IPMP (59.26 %), and MD-IPMP (56.93 %) (Table 1). The high microwave power in MD elevated the product temperature, leading to the conversion of some polysaccharides into oligosaccharides or caramelized compounds through Maillard and caramelization reactions (Tian et al., 2016), which likely accounts for the lower neutral sugar content in MD-IPMP. In contrast, MVD-IPMP preserved the highest neutral sugar levels due to relatively lower drying temperatures, which reduce the activity of polysaccharide-degrading enzymes (An et al., 2022). Additionally, enhanced microwave power during MVD may further increase neutral sugar content, as observed in studies on okra (*Abelmoschus esculentus*) (Yuan, He, Xiang, Huang, et al., 2020) and loquat leaves polysaccharides (Fu et al., 2020). Table 1 also indicates that MVD-IPMP had the highest uronic acid content at 30.74 %, with MD-IPMP, IRD-IPMP, and HD-IPMP following at 25.75 %, 24.05 %, and 23.87 %, respectively. This suggests that drying methods significantly influence uronic acid content ($p < 0.05$). The levels of glucuronic and galacturonic acids are significantly influenced by the activities of glucuronidase and galacturonic acid enzymes, which function optimally between 50 and 80 °C (An et al., 2022). Reduced temperatures and oxygen levels in MVD decrease enzyme activity, enhancing uronic acid retention. Moreover, thermal and oxidative processes significantly contribute to the reduced retention of uronic acids in IRD-IPMP and HD-IPMP due to the higher temperatures and

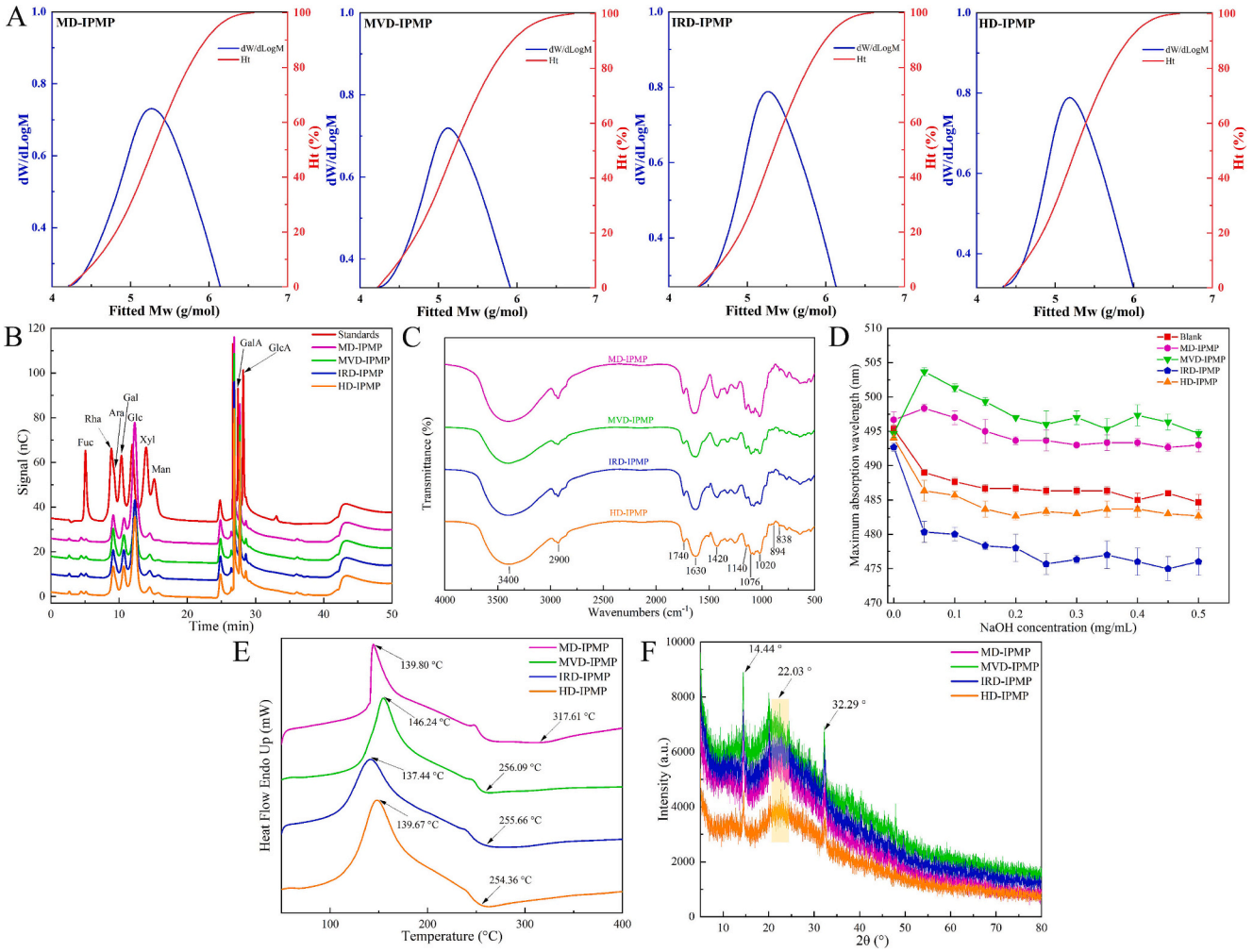

Fig. 2. (A) Molecular weight distribution curves of IPMPs; (B) HPAEC chromatograms of IPMPs; (C) FT-IR spectra of IPMPs; (D) Congo red test results of IPMPs; (E) DSC curves of IPMPs; (F) XRD spectra of IPMPs. (For interpretation of the references to colour in this figure legend, the reader is referred to the web version of this article.)

increased oxygen exposure involved in these methods (Chen et al., 2019a). Residual protein levels remained between 3.72 % and 5.09 % across all samples, even after effective deproteinization. The residual protein in the extracted polysaccharides is probably due to protein-polysaccharide complexes, aligning with earlier research that identified a 4.48 % protein content in IPM cake meal polysaccharides (Shi et al., 2024). Among the four samples, MVD-IPMP exhibited the highest protein content, likely because the lower temperatures during MVD drying help preserve proteins and prevent denaturation.

3.1.3. The distribution of molecular weights for IPMPs

The weight-average molecular weight (*Mw*), number-average molecular weight (*Mn*), and polydispersity index (PDI = *Mw*/*Mn*) of four IPMPs were assessed using HPGPC. The results are presented in Table 1 and Fig. 2A. The HPGPC chromatograms of the four IPMPs are shown in Fig. S3. The *Mw* values for MD-IPMP, MVD-IPMP, IRD-IPMP, and HD-IPMP were approximately 370.67 ± 9.99 kDa, 346.26 ± 10.83 kDa, 396.27 ± 5.63 kDa, and 337.87 ± 6.72 kDa, respectively ($p < 0.05$). Notably, HD-IPMP exhibited the lowest *Mw*, which is likely due to structural disruption and thermal degradation of the polysaccharides induced by the high temperatures during hot air drying (Yuan et al., 2020). Previous studies have shown that elevated temperatures can enhance polysaccharide production, but they also lead to a significant reduction in molecular weight due to degradation (Su et al., 2017). In contrast, IRD-IPMP exhibited the highest *Mw*, potentially due to the removal of part of the polysaccharide hydration layer during infrared drying, which promotes structural aggregation (Wang et al., 2019). Although both MD-IPMP and MVD-IPMP were subjected to microwave drying, MVD-IPMP exhibited a lower *Mw*. This discrepancy is likely due to the higher microwave energy in the MVD process, which leads to more extensive breakage of polysaccharide chains, increasing thermal degradation and hydrolysis (Zeng et al., 2024) This is consistent with studies on okra polysaccharides, which showed that higher microwave power resulted in a decrease in *Mw* (Yuan et al., 2020). These findings underscore the substantial influence of drying techniques on the molecular weight of IPMPs, as documented in prior research (An et al., 2022; Zeng et al., 2024). The PDI indicates the range of molecular weight distribution, where lower values signify a more uniform distribution (Xiong et al., 2022). The PDI values for the four IPMPs ranged from 3.13 to 3.92, indicating a relatively narrow molecular weight distribution and suggesting that these polysaccharides are molecularly homogeneous (Deng et al., 2020). HD-IPMP exhibited the lowest PDI (3.13), indicating high homogeneity, likely due to degradation induced by high temperatures during drying. In contrast, MVD-IPMP exhibited the highest PDI (3.92), reflecting a broader molecular weight distribution with less thermal aggregation. These findings highlight the significant impact of drying methods on the molecular weight distribution of polysaccharides.

3.1.4. The monosaccharide composition of IPMPs

The HPAEC chromatograms and molar ratios of the monosaccharide compositions for the four IPMPs are shown in Fig. 2B and Table 1, respectively. The analysis revealed that all four IPMPs contained nine monosaccharides: rhamnose (Rha), fucose (Fuc), glucose (Glc), arabinose (Ara), xylose (Xyl), galactose (Gal), mannose (Man), glucuronic acid (GlcA), and galacturonic acid (GalA). However, notable differences in molar ratios were observed, suggesting that the drying methods significantly influenced the distribution of monosaccharides. Specifically, MD-IPMP exhibited the highest Glc content (51.27 %, $p < 0.05$), while MVD-IPMP showed the highest concentrations of Rha (11.22 %), Ara (12.03 %), Gal (12.18 %), and GalA (32.34 %) ($p < 0.05$). In contrast, MD-IPMP contained the lowest GalA content (25.06 %), whereas the MVD method appeared to preserve GalA more efficiently. These findings align with previous studies suggesting that drying methods impact monosaccharide composition (Li et al., 2021; Wang et al., 2019). Variations in drying techniques can alter monosaccharide proportions, potentially due to changes in temperature and oxygen exposure (Liu et al., 2020). For example, MVD treatment of *Rosa sterilis* fruit polysaccharides increased GalA and Gal levels while decreasing Man (Chen, Sun, Dai, et al., 2024). Similarly, MVD-treated polysaccharides from *Rosa roxburghii* Tratt fruit exhibited higher levels of GalA and Ara (Zhang et al., 2024), consistent with the results obtained for MVD-IPMP. The composition and relative abundance of monosaccharides are known to significantly affect the biological activity of polysaccharides (Yuan et al., 2020). Therefore, assessing the biological activities of IPMPs prepared with different drying methods is crucial.

3.2. The structure characterizations of different IPMPs

3.2.1. FT-IR spectroscopy

Fig. 2C displays the FT-IR spectra for the four IPMPs. Although the overall spectral patterns of these polysaccharides are similar, the intensities of their characteristic peaks differ. The absorption band at approximately 3400 cm^{-1} signifies O—H stretching vibrations, while the peak near 2900 cm^{-1} is indicative of C—H bending vibrations, both characteristic of carbohydrate compounds (Deng et al., 2020; Yang, Luo, Sang, & Kan, 2022). The 1740 cm^{-1} signal indicates symmetric stretching of esterified carboxyl groups (Li et al., 2021b). The absorption bands near 1630 and 1420 cm^{-1} indicate the asymmetric stretching and vibration of carboxyl groups, verifying the presence of uronic acids in the polysaccharides. The 1200–1000 cm^{-1} region mainly features ring vibrations and C-O-C and C-O-H bond stretching. Absorption bands at 1140, 1076, and 1020 cm^{-1} suggest the presence of pyran-type glycosidic bonds (Chen, Sun, Chen, et al., 2024). Below 1000 cm^{-1}, distinct peaks at approximately 894 and 838 cm^{-1} correspond to the β- and α-configurations of glycosidic linkages, respectively (Xiong et al., 2022). Overall, the FT-IR spectra show that all four IPMPs share similar backbone structures and chemical groups, suggesting that the different drying techniques did not significantly affect the structural integrity of the polysaccharides.

3.2.2. Triple-helical structure examination

A Congo red assay was conducted to assess the existence of a triple-helical structure. The principle of this assay relies on the formation of a stable complex between Congo red and triple-helix polysaccharides, which causes an increase in the maximum absorption wavelength (λ_{max}) under weakly alkaline conditions. As the concentration of NaOH is increased, the helical structure of the polysaccharide is disrupted, resulting in a significant decrease in λmax. Therefore, monitoring the changes in λmax of the polysaccharide-Congo red complex at different sodium hydroxide concentrations can effectively be used to identify the presence of a triple-helix structure in the polysaccharide (Tan et al., 2021). Fig. 2D shows the results of the Congo red assay for the four IPMPs. MD-IPMP and MVD-IPMP showed a significant red shift in λmax at NaOH concentrations below 0.1 mol/L, indicating that their triple-helix structures were maintained after the MD and MVD drying processes. In contrast, IRD-IPMP and HD-IPMP did not display a red shift, indicating that their triple-helix structures were disrupted by the IRD and HD drying methods. These observations may be attributed to changes in molecular weight and monosaccharide composition caused by the different drying conditions. This finding is consistent with previous studies (Chen et al., 2019a), highlighting the impact of drying methods on the structural integrity of polysaccharides.

3.2.3. Thermal stability analysis

Thermal stability is a crucial physicochemical property of polysaccharides, especially for their industrial and commercial applications. DSC is a widely used technique for evaluating the thermal behavior of these compounds (Munir et al., 2016). Fig. 2E displays the DSC curves, while Table 1 provides the associated thermal parameters for the IPMPs within the 50–400 °C temperature range. The DSC profiles of all four IPMP samples showed both endothermic and exothermic peaks. Key

thermal parameters such as onset temperature (*To*), melting temperature (*Tm*), melting enthalpy (Δ*Hm*), degradation temperature (*Tg*), and degradation enthalpy (Δ*Hg*) were derived from these peaks, as shown in Table 1. The *Tm* values of the IPMPs ranged from 137.44 °C to 146.24 °C, likely due to the release of residual water or the breakdown and dehydroxylation of polysaccharide chains at these temperatures (Mannai et al., 2023; Mohammed et al., 2020). MD-IPMP exhibited a sharper exothermic peak, indicating a narrower melting range and a more concentrated molecular weight distribution (Deng et al., 2020). Furthermore, MD-IPMP showed the highest *Tg* at 317.61 °C, significantly higher than the other samples ($p < 0.05$). This suggests that MD-IPMP has enhanced thermal stability, likely due to the degradation of heat-resistant components during the drying process. These findings highlight the crucial influence of drying techniques on the thermal stability of IPMPs.

3.2.4. XRD analysis

The crystallinity of polysaccharides significantly influences their flexibility, swelling behavior, solubility, and various physical properties. XRD is the standard technique for evaluating the crystallinity and crystallization properties of polysaccharides. Fig. 2F presents the XRD patterns of the four IPMPs. All four IPMP samples exhibited diffraction peaks at 14.44°, 22.03°, and 32.29° 2θ, but no significant absorption peaks. This pattern indicates that the IPMPs are semi-crystalline polymers. Notably, HD-IPMP exhibited lower peak intensities than the other samples, indicating reduced crystallinity. This suggests that HD may lead to a more amorphous structure in the polysaccharides by altering their crystallization properties. Similar results have been reported for polysaccharides derived from *Rosa roxburghii* Tratt fruit (Zhang et al., 2024).

3.2.5. Morphological characterizations

Fig. 3 presents the surface morphologies of the four IPMPs observed under SEM at magnifications of 100×, 5000×, and 10,000×. At 100× magnification, all samples displayed a sheet-like structure. However, MD-IPMP, IRD-IPMP, and HD-IPMP showed a mixture of sheets and thin fragments, while MVD-IPMP exhibited larger sheet-like structures, likely due to the crosslinking and aggregation of uronic acids (Li et al., 2024). At higher magnifications (5000× and 10,000×), MD-IPMP and MVD-IPMP exhibited similar morphological features, including numerous spherical particles forming a network structure, which became more pronounced at higher magnifications. Despite these similarities, some differences were observed: MVD-IPMP particles were uniform in size and regularly arranged, while MD-IPMP contained rod-like particles with more pronounced particle aggregation. Both MD-IPMP and MVD-IPMP exhibited close connections between spheres, suggesting well-connected and less damaged polysaccharide chains, consistent with the findings from the Congo red analysis. In contrast, HD-IPMP and IRD-IPMP showed clustered bulge formations. These formations may result from temperature gradients and opposing moisture flow directions during HD, causing the granules in HD-IPMP to contract and rise. For IRD-IPMP, rapid infrared radiation likely hindered effective moisture evaporation, leading to the accumulation of internal water and the subsequent aggregation of polysaccharides into bulge-like structures (An et al., 2022). These morphological observations confirm that the drying method significantly influences the structure and microstructure of IPMPs. Such structural differences are expected to impact their physicochemical properties and biological activities.

3.3. In vitro inhibition of non-enzymatic glycation of different IPMPs

Non-enzymatic glycation, a Maillard reaction occurring in the body, initiates when a reducing sugar's carbonyl group reacts with a protein's free amino group, producing a Schiff base. As displayed in Fig. 4A, the Schiff base undergoes rearrangement to form Amadori products, such as fructosamine, which are further transformed into α-dicarbonyl compounds, including methylglyoxal, glyoxal, and 3-deoxyglucosone. These intermediates undergo dehydration, cyclization, and oxidation, ultimately forming AGEs, irreversible compounds linked to oxidative stress, inflammation, thrombosis, and fibrosis (Dou et al., 2021). AGEs are pivotal in the development of diabetic vascular complications (Spínola et al., 2020). Strategies targeting the reduction or inhibition of AGEs

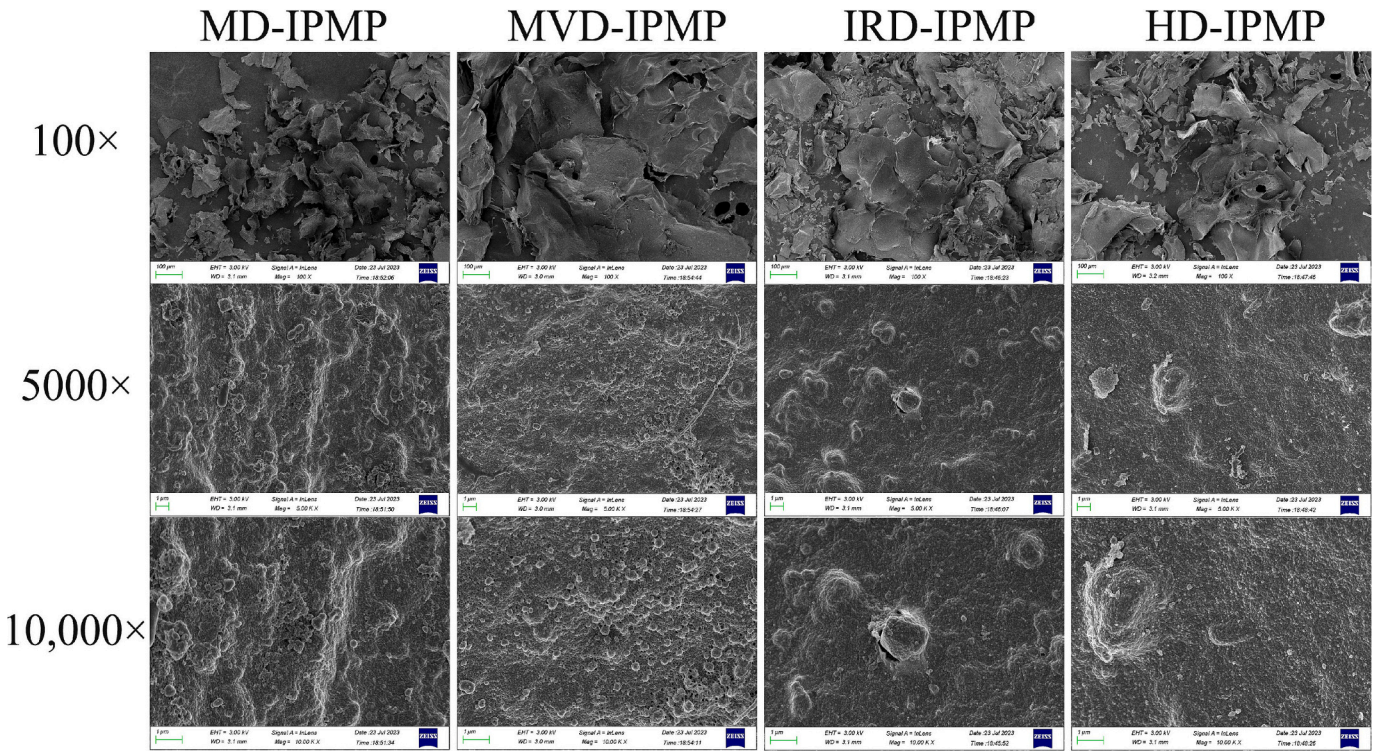

Fig. 3. SEM images of IPMPs at magnifications of 100×, 5000× and 10,000 × .

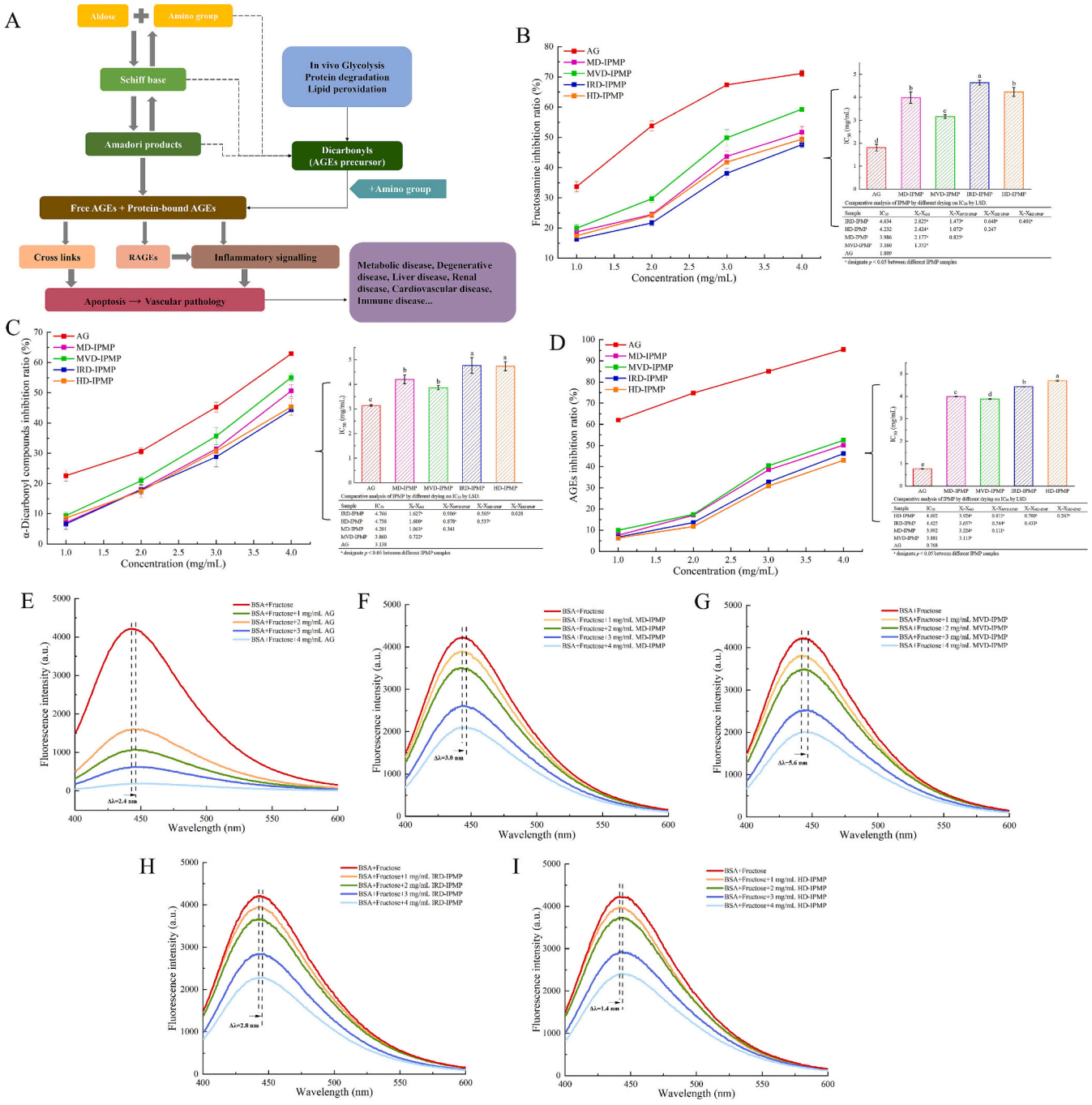

Fig. 4. (A) Non-enzymatic protein glycosylation pathways leading to the formation of advanced glycation end products (AGEs) and their role in diabetes complications pathogenesis; RAGE: receptor for advanced glycation end products; (B) Inhibition of fructosamine by IPMPs; (C) Inhibition of α-dicarbonyl compounds by IPMPs; (D) Inhibition of AGEs by IPMPs; (*E*-I) Fluorescence spectra of AGEs with increasing concentrations of IPMPPs and AG.

formation hold promise for mitigating diabetic complications (Amamou et al., 2020). This study evaluated the anti-glycation potential of four IPMPs using a BSA-fructose model, measuring key products at three glycation stages: fructosamine (stage I), α-dicarbonyl compounds (stage II), and AGEs (stage III).

In Fig. 4B, the fructosamine inhibitory activities (y) of the four IPMPs exhibited a quadratic relationship with concentration (x) ($p < 0.05$). The derived equations were: MD-IPMP, $y = 2.321\ x^2 + 0.213x + 15.975$ ($R^2 = 0.962$); MVD-IPMP, $y = 1.018\ x^2 + 8.160x + 10.403$ ($R^2 = 0.997$); IRD-IPMP, $y = 2.056\ x^2 + 0.336x + 13.837$ ($R^2 = 0.991$); HD-IPMP, $y = 3.167\ x^2$–$2.013x + 16.160$ ($R^2 = 0.967$). The IC_{50} values for fructosamine inhibition were 3.986 mg/mL (MD-IPMP), 3.160 mg/mL (MVD-IPMP), 4.634 mg/mL (IRD-IPMP), and 4.232 mg/mL (HD-IPMP). Among the four IPMPs, MVD-IPMP demonstrated the strongest inhibitory effect on fructosamine, although it remained less effective than AG (IC_{50}: 1.809 mg/mL). During the intermediate phase, fructosamine undergoes dehydration, rearrangement, and other reactions, yielding reactive two-carbon compounds. Studies indicate that dicarbonyl compounds rapidly form AGEs by cross-linking proteins, with approximately 45–50 % of AGEs derived from α-dicarbonyl compounds (Zhu et al., 2019). Fig. 4C illustrates the inhibition rates of α-dicarbonyl compounds generated at this stage. The inhibitory activities (y) of α-dicarbonyl compounds for the four IPMPs showed significant quadratic concentration (x)-dependent relationships ($p < 0.05$). The equations were: $y =$

$2.137\,x^2 + 3.653x + 1.386$ ($R^2 = 0.999$); $y = 1.878\,x^2 + 5.830x + 1.693$ ($R^2 = 0.999$); IRD-IPMP, $y = 0.811\,x^2 + 8.474x$ - 2.545 ($R^2 = 0.999$); and HD-IPMP, $y = 1.431\,x^2 + 5.225x + 1.933$ ($R^2 = 0.999$). The IC_{50} values for α-dicarbonyl compound inhibition were ranked as follows: IRD-IPMP (4.766 mg/mL) > HD-IPMP (4.738 mg/mL) > MD-IPMP (4.201 mg/mL) > MVD-IPMP (3.860 mg/mL) > AG (3.138 mg/mL). The IPMPs were less effective than AG at suppressing intermediates during glycation. MVD-IPMP demonstrated significant inhibition, likely due to its elevated uronic acid content and reduced molecular weight. Uronic acid, capable of reducing reactive oxygen species and inhibiting glycosylated protein oxidation, plays a pivotal role in reducing fructosamine formation and limiting α-dicarbonyl compound production (Li et al., 2023).

In the final phase, fluorescent AGEs were identified as the endpoint products. The AGEs inhibitory activities (y) of the four IPMPs exhibited a quadratic concentration-dependent pattern ($p < 0.05$), with the following equations: MD-IPMP, $y = 0.261\,x^2 + 13.660x$ - 8.576 ($R^2 = 0.990$); MVD-IPMP, $y = 3.341\,x^2$–$1.071x + 6.569$ ($R^2 = 0.958$); IRD-IPMP, $y = 1.167\,x^2 + 8.080x$ - 3.457 ($R^2 = 0.980$); HD-IPMP, $y = -0.403\,x^2 + 15.248x$ - 11.390 ($R^2 = 0.985$) (Fig. 4D). The IC_{50} values for AGEs inhibition were 3.992 mg/mL (MD-IPMP), 3.881 mg/mL (MVD-IPMP), 4.425 mg/mL (IRD-IPMP), 4.692 mg/mL (HD-IPMP), and 0.768 mg/mL (AG) ($p < 0.05$). While MVD-IPMP exhibited the strongest AGEs inhibition among the IPMPs, its efficacy remained lower than that of AG. Its elevated uronic acid content and relatively lower molecular weight likely enhance its interactions with glycation intermediates, thus impeding their conversion into AGEs. Similar observations have been reported in studies on polysaccharides from *Rosa sterilis* fruits (Chen, Sun, Dai, Sun and Hu, 2024). The chelating properties of uronic acid may inhibit glycation by binding to catalytic metal ions or directly interacting with AGEs receptors, thereby preventing AGEs formation (Bhuiyan et al., 2017; Li et al., 2023). Additionally, reduced molecular weight may improve its capacity to target glycation intermediates (Katz et al., 2010). These findings indicate that MVD-IPMP, owing to its unique composition, is a promising glycation inhibitor for managing diabetic complications.

Fig. 4E-I depict the fluorescence intensity changes in the BSA-fructose system following IPMPs addition. The system showed enhanced fluorescence intensity at 360 nm after 24 h of incubation at 50 °C, suggesting the formation of AGEs. A concentration-dependent decrease in fluorescence was observed with the addition of IPMPs or AG, confirming their inhibitory potential. Furthermore, the system's maximum absorption peak exhibited a redshift upon IPMPs/AG addition: MD-IPMP, 443.4 to 446.4 nm; MVD-IPMP, 441.2 to 446.8 nm; IRD-IPMP, 442.8 to 445.6 nm; HD-IPMP, 441.6 to 443.0 nm; and AG, 445.2 to 447.6 nm. This redshift indicates increased polarity surrounding the fluorophore. Similar findings were reported in studies on *Gelidium amansiis* polysaccharide (Yu et al., 2021), further supporting the conclusion that IPMPs inhibit glycation at multiple stages.

3.4. Antioxidant activity of different IPMPs in a linoleic acid system

Lipids, the primary components of cell membranes, undergo peroxidation that can disrupt membrane structure and function. MDA, a primary byproduct of lipid oxidation, serves as a standard indicator for lipid peroxidation (Ma et al., 2021). The TBA method was employed to measure MDA content in the oxidized system with linoleic acid as the substrate, assessing the inhibitory effects of IPMPs on linoleic acid peroxidation. As shown in Fig. 5A, the antioxidant activity of the four IPMPs significantly increased with concentrations ranging from 0.125 to 5 mg/mL against linoleic acid oxidation. The inhibitory activities (y) of MD-IPMP, MVD-IPMP, IRD-IPMP, and HD-IPMP exhibited quadratic concentration (x)-dependent patterns ($p < 0.05$), described by the equations: $y = -2.199\,x^2 + 17.689x + 40.683$ ($R^2 = 0.963$), $y = -1.846\,x^2 + 16.832x + 31.715$ ($R^2 = 0.974$), $y = -3.108\,x^2 + 22.826x + 28.773$ ($R^2 = 0.983$), and $y = -2.651\,x^2 + 22.319x + 24.834$ ($R^2 = 0.974$), respectively. Compared to Vc with an IC_{50} of 0.026 mg/mL, the four IPMPs exhibited lower potency. Nonetheless, they still displayed significant inhibitory effects, with IC_{50} values recorded as 0.832 mg/mL (MD-IPMP), 0.495 mg/mL (MVD-IPMP), 0.841 mg/mL (IRD-IPMP), and 1.073 mg/mL (HD-IPMP). At a concentration of 5 mg/mL, the inhibitory capacities were 71.10, 74.52, 71.07, and 69.84 % for MD-IPMP, MVD-IPMP, IRD-IPMP, and HD-IPMP, respectively. The findings demonstrated MVD-IPMP's exceptional resistance to linoleic acid oxidation compared to other drying methods assessed. The increased activity of MVD-IPMP can be attributed to its reduced molecular weight and elevated uronic acid content. Polysaccharides are known for neutralizing free radicals by donating electrons or hydrogen atoms. The presence of uronic acid groups in these molecules facilitates interactions with the hydrogen atoms on the anomeric carbon. Electrophilic groups like keto or aldehyde functionalities can facilitate hydrogen release from hydroxyl bonds, particularly in acidic environments. Thus, polysaccharides high in uronic acid generally demonstrate significant antioxidant properties (Chaouch et al., 2015). Furthermore, polysaccharides with lower molecular weights have more reductive hydroxyl groups, increasing their capacity to neutralize free radicals and enhance antioxidant activity (Chen et al., 2019). These findings suggest that IPMPs effectively suppress linoleic acid peroxidation and hold promise as oxidation-blocking agents for lipid-based applications.

3.5. In vitro evaluation of hypoglycemic activity of different IPMPs

3.5.1. In vitro α-glucosidase inhibitory activity

α-Glucosidase plays a vital role in starch digestion within the small intestine by hydrolyzing α-1,4 glycosidic bonds in oligosaccharides, thereby releasing glucose. Inhibiting it may slow carbohydrate digestion, lower postprandial blood glucose spikes, and help prevent diabetes (Amamou et al., 2020). Fig. 5B presents the α-glucosidase inhibition profiles of the four IPMPs, with acarbose as a reference. All IPMPs exhibited concentration (x)-dependent quadratic inhibition (y) ($p < 0.05$), described by the following equations: $y = -0.779\,x^2 + 11.272x + 30.921$ ($R^2 = 0.992$) for MD-IPMP, $y = -1.380\,x^2 + 15.378x + 23.322$ ($R^2 = 0.990$) for MVD-IPMP, $y = -0.654\,x^2 + 10.661x + 25.116$ ($R^2 = 0.990$) for IRD-IPMP, and $y = -0.702\,x^2 + 11.003x + 27.474$ ($R^2 = 0.990$) for HD-IPMP. The ranking based on IC_{50} values was as follows: MVD-IPMP (1.719 mg/mL) > MD-IPMP (1.814 mg/mL) > HD-IPMP (2.153 mg/mL) > IRD-IPMP (2.592 mg/mL) > acarbose (0.109 mg/mL). MVD-IPMP exhibited the most potent inhibitory effect among the four IPMPs evaluated, attributed to its smaller molecular weight and higher uronic acid level. Research indicates that polysaccharides with lower molecular weights and higher uronic acid level are more effective at inhibiting α-glucosidase, as these characteristics facilitate improved access to the enzyme's active sites (Zheng, Jia, Luo, et al., 2022). Furthermore, higher levels of arabinose and xylose are associated with more effective inhibition (Wang et al., 2023). Additionally, the presence of glucose and triple-helical structure has been shown to further enhance inhibitory potential (Chen, Zhang, Yang, et al., 2024). The triple-helix structure of polysaccharides is stabilized through hydrogen bonds and hydrophobic interactions, which significantly enhance their resistance to degradation in physiological environments (Xiong et al., 2019). This increased stability not only protects the polysaccharides from enzymatic or chemical breakdown but also prolongs their functional activity within the body. These structural features likely contribute to the superior α-glucosidase inhibition observed with MVD-IPMP. In summary, IPMPs, particularly MVD-IPMP, exhibit significant potential as hypoglycemic agents. Further investigation into their inhibitory kinetics and specific interaction mechanisms with α-glucosidase is warranted.

3.5.2. Inhibitory kinetics analysis

Lineweaver–Burk plots were used to study the α-glucosidase inhibition mechanism by IPMPs. Reaction rates were assessed at *p*NPG concentrations of 1–4 mM and IPMP concentrations of 1, 4, and 6 mg/mL (Fig. 5C–F). The kinetic parameters obtained from these analyses are

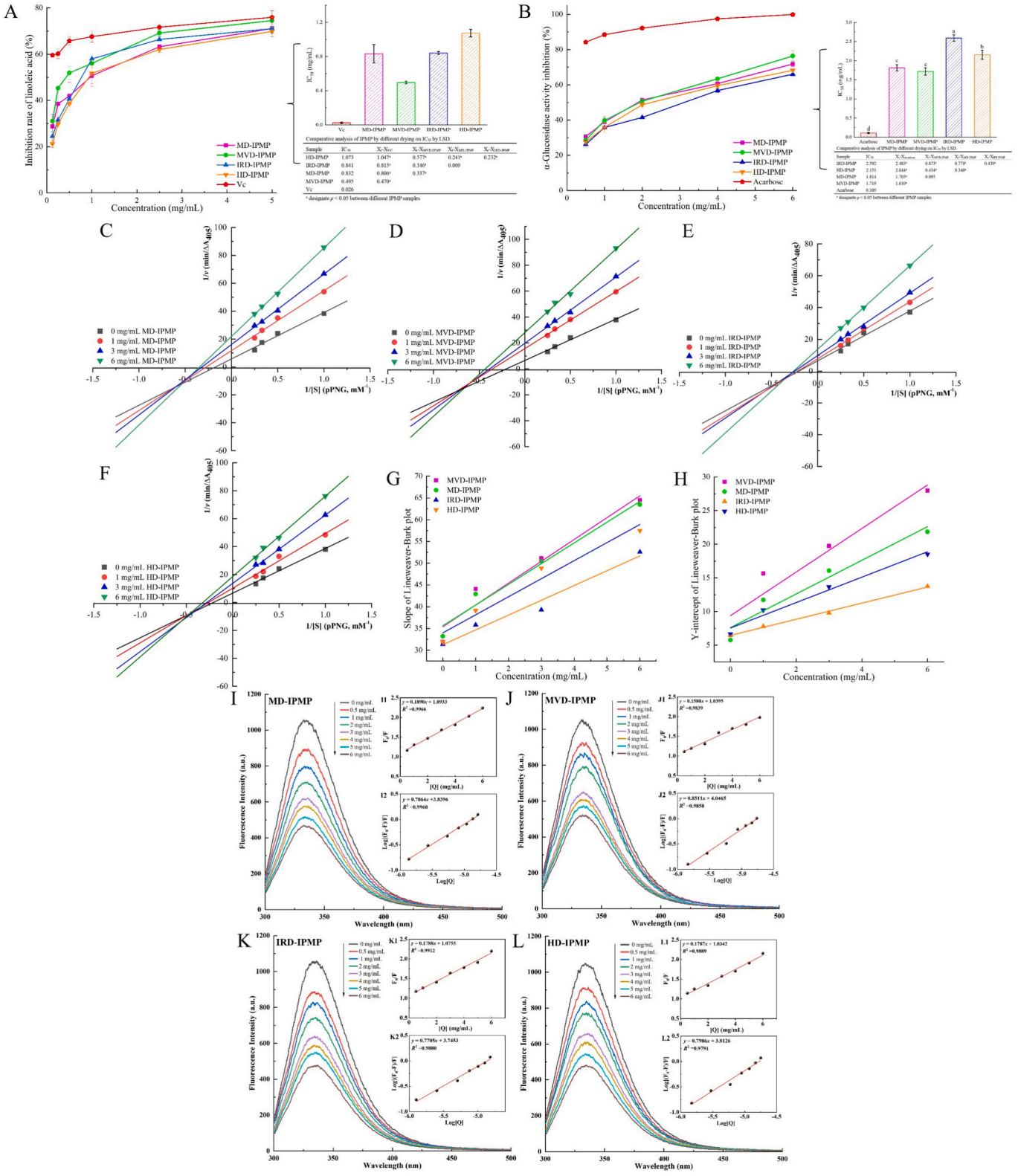

Fig. 5. (A) Inhibitory activity against linoleic acid oxidation; (B) Inhibitory activity against α-glucosidase; (C—F) Lineweaver–Burk plots versus IPMPs concentration; (G) Slope of the Lineweaver–Burk plot versus IPMPs concentration; (H) Y-intercept of the Lineweaver–Burk plot versus IPMPs concentration; (I–L) Fluorescence spectra of α-glucosidase in the presence of IPMPs at varying concentrations; the Stern–Volmer plots for the interaction between α-glucosidase and different concentrations of MD-IPMP (I1), MVD-IPMP (J1), IRD-IPMP (K1), and HD-IPMP (L1); the double logarithm regression plots of log $[(F_0 - F)/F]$ versus log[Q] for α-glucosidase with increasing concentrations of MD-IPMP (I2), MVD-IPMP (J2), IRD-IPMP (K2), and HD-IPMP (L2).

Table 2a
Inhibitory kinetic parameters of α-glucosidase after interaction with different IPMPs.

Sample	Concentration (mg/mL)	K_m (mM)	V_{max} (ΔA405/min)	K_i (mg/mL)	K_{is} (mg/mL)	K_{is}/K_i	K_q (M^{-1} s^{-1})	K_{SV} (M^{-1})	K_a (M^{-1})	n
MD-IPMP	0	5.77	0.17	7.48	3.04	0.41	7.00×10^{12}	7.00×10^{4}	6.91×10^{3}	0.79
	1	3.66	0.08							
	3	3.14	0.06							
	6	2.54	0.04							
MVD-IPMP	0	4.91	0.15	7.06	2.90	0.41	5.49×10^{12}	5.49×10^{4}	1.11×10^{4}	0.85
	1	2.81	0.06							
	3	2.59	0.05							
	6	2.31	0.04							
IRD-IPMP	0	4.86	0.15	9.20	5.38	0.59	7.08×10^{12}	7.08×10^{4}	5.56×10^{3}	0.77
	1	4.60	0.13							
	3	4.01	0.10							
	6	3.83	0.07							
HD-IPMP	0	4.78	0.15	7.70	4.00	0.52	6.04×10^{12}	6.04×10^{4}	6.50×10^{3}	0.80
	1	3.83	0.10							
	3	3.58	0.07							
	6	3.10	0.05							

summarized in Table 2a. Without IPMPs, the K_m values of α-glucosidase ranged from 4.78 to 5.77 mM, and V_{max} values ranged from 0.15 to 0.17 ΔA_{405}/min. The addition of IPMPs reduced both K_m and Vmax, indicating mixed-type inhibition. Moreover, Double-reciprocal (Lineweaver–Burk) plots intersected in the third quadrant, indicating that IPMPs compete for the active site while also binding to the enzyme-substrate complex to form a ternary complex (IPMP–enzyme–substrate) (Wang et al., 2020). The binding strength was quantified through K_i and K_{is} values, calculated by plotting slopes and intercepts of the Lineweaver–Burk data against IPMP concentrations (Chen et al., 2024) (Fig. 5G–H). Table 2a indicates that all IPMPs exhibit significantly lower K_{is} values compared to their K_i values ($K_{is}/K_i < 1$), suggesting a stronger binding affinity to the enzyme-substrate complex than to the free enzyme (Zheng, Jia, Luo, et al., 2022). MVD-IPMP exhibited the lowest K_i (7.06 mg/mL), K_{is} (2.90 mg/mL), and K_{is}/K_i (0.41) among the four IPMPs, indicating its strong affinity and enhanced inhibitory activity against α-glucosidase. These results highlight the potential of MVD-IPMP as a promising hypoglycemic agent.

3.5.3. *Interaction mechanism between IPMPs and α-glucosidase*

3.5.3.1. Impact of IPMPs on the fluorescence properties of α-glucosidase. Proteins with aromatic amino acids, such as tyrosine and phenylalanine, fluoresce when excited at 280 nm, a phenomenon known as endogenous protein fluorescence (Jia et al., 2021). Inhibitor binding to α-glucosidase can alter the polarity of tyrosine and tryptophan residues, leading to their unfolding. This unfolding decreases fluorescence intensity by quenching the fluorescence signal (Guo, Yin, et al., 2023). Thus, monitoring changes in fluorescence allows direct observation of alterations in the enzyme's structure and environment. Fluorescence intensity was measured at various IPMP concentrations to explore the interaction between α-glucosidase and IPMPs. As shown in Fig. 5I-L, a progressive decrease in fluorescence intensity with increasing IPMP concentrations indicates the interaction between α-glucosidase and the four IPMPs. The maximum fluorescence emission wavelength shifted to longer wavelengths with increasing IPMP concentration. Specifically, the shifts were: MD-IPMP from 338 nm to 340 nm, MVD-IPMP from 335 nm to 339 nm, IRD-IPMP from 337 nm to 339 nm, and HD-IPMP from 336 nm to 339 nm. These shifts suggest that the interaction between IPMPP and α-glucosidase alters the polarity surrounding the tyrosine and tryptophan residues, shifting the microenvironment from hydrophilic to hydrophobic. Such structural changes may cause the fluorescent residues to unfold, resulting in a decrease in fluorescence (Jia et al., 2020).

In general, fluorescence quenching typically occurs through two primary mechanisms: static quenching, where a non-fluorescent complex forms between the fluorophore and the quencher, and dynamic quenching, which results from energy transfer due to molecular collisions (Zhao et al., 2021). To determine the quenching mechanism, fluorescence quenching data were analyzed using the Stern-Volmer equation (Eq. (9)). The Stern-Volmer plots (Fig. 5I1–L1), which depict the interaction between α-glucosidase and the four IPMPs, reveal a clear linear relationship with high regression coefficients ($R^2 > 0.98$), indicating strong enzyme-polysaccharide interactions. The maximum dynamic quenching rate constant for biological macromolecules interacting with various quenchers is typically 2.0×10^{10} $L \bullet M^{-1} S^{-1}$. When the quenching rate constant (K_q) exceeds this threshold, static quenching dominates (Zheng, Jia, Luo, et al., 2022). The calculated K_q values for MD-IPMP, MVD-IPMP, IRD-IPMP and HD-IPMP were 7.00×10^{12}, 5.49×10^{12}, 7.08×10^{12}, and 6.04×10^{12} M^{-1} s^{-1}, respectively (Table 2a), all exceeding the threshold, indicating that static quenching predominates. The quenching mechanism was further examined by K_a and n from the slope and intercept of the plot of $\log[(F_0—F)/F]$ versus $\log[Q]$ (Wang et al., 2018). The K_a values, derived from Fig. 5I2–L2, were 6.91×10^3, 1.11×10^4, 5.56×10^3 and 6.50×10^3 M^{-1} for MD-IPMP, MVD-IPMP, and IRD-IPMP and HD-IPMP, respectively (Table 2a), indicating that MVD-IPMP exhibits the strongest binding affinity for α-glucosidase. The n values, similar for all four IPMPs, indicate that the enzyme binds to a similar class of binding sites for each polysaccharide, with values ranging from 0.77 to 0.85 (Table 2a). This observation aligns with previous studies on *I. polycarpa* Maxim polysaccharides, where n values close to 1 have also been reported (Shi et al., 2025). In conclusion, the comprehensive analysis of fluorescence data reveals that MVD-IPMP has the strongest binding affinity for α-glucosidase, consistent with its higher inhibitory potency observed in kinetic and inhibitory rate studies.

3.5.3.2. Conformational change analysis. Aromatic amino acids, such as tryptophan and tyrosine, show shifts in their absorption wavelengths when interacting with α-glucosidase. Structural changes in the enzyme upon binding with polysaccharides can be detected by ultraviolet (UV) spectroscopy (Fei et al., 2014). As shown in Fig. 6A–D, the four IPMPs cause a marked increase in absorbance at higher concentrations, along with a slight blue shift. This suggests the formation of an enzyme-inhibitor complex, inducing structural changes in the enzyme. Similar blue shifts in UV absorption have been observed in polysaccharide-enzyme interactions, such as those involving Prickly pear polysaccharides (Wang et al., 2018), whereas a red shift was observed when α-glucosidase binds to RP-SeNPs-1 (Zhao et al., 2023). The structural features of the four IPMPs—especially hydroxyl and carboxyl groups—facilitate non-covalent interactions (e.g., hydrogen bonding and hydrophobic interactions) with α-glucosidase, contributing to enzyme inhibition. Moreover, the presence of uronic acid in IPMPs may alter the environment surrounding the tryptophan and tyrosine residues, inducing conformational changes in the enzyme (Shi et al., 2025). These

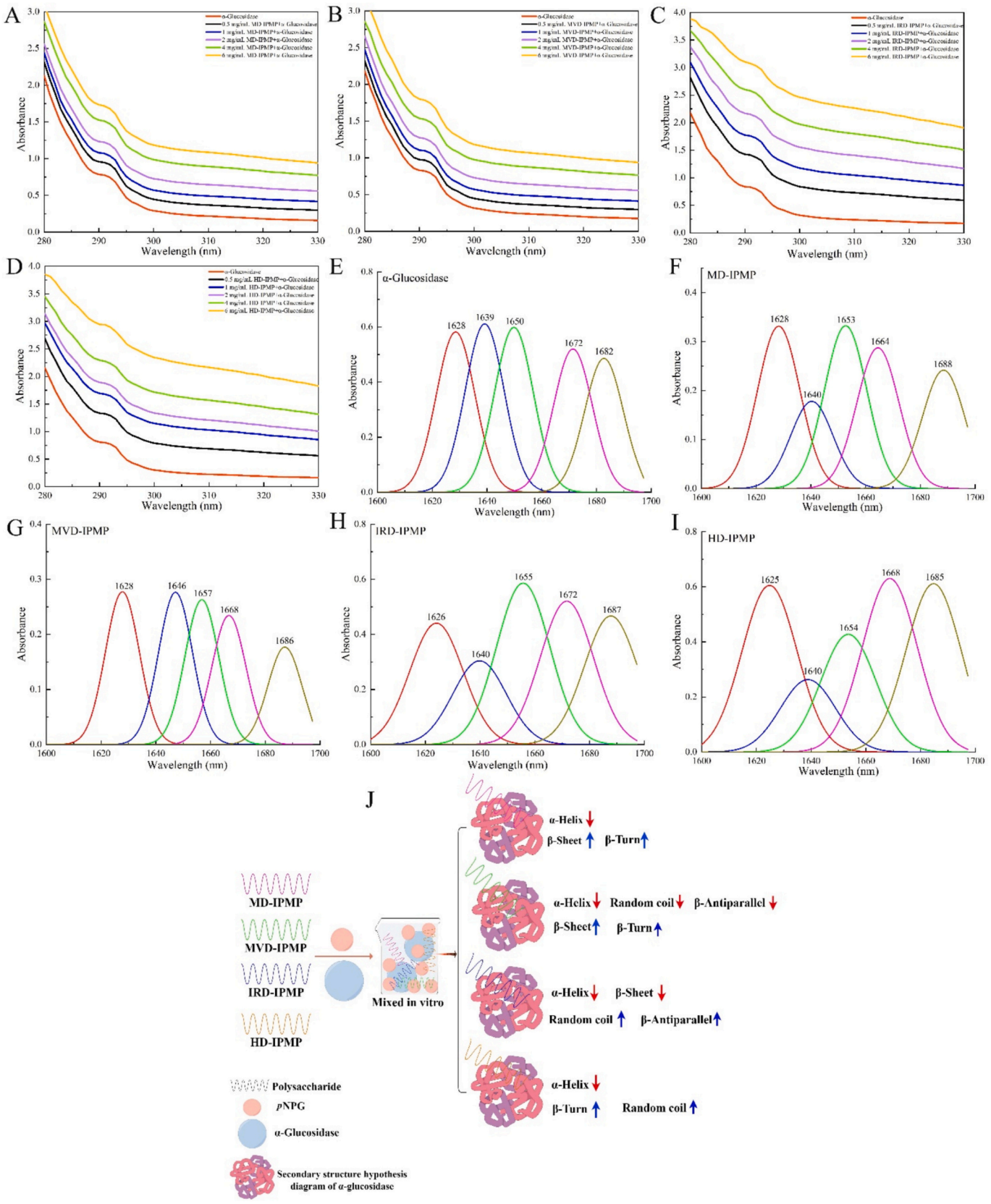

Fig. 6. UV absorbance spectra for α-glucosidase in the presence of MD-IPMP (A), MVD-IPMP (B), IRD-IPMP (C), and HD-IPMP (D) at concentrations ranging from 0.5 to 5.0 mg/mL; The curve-fitted amide I bands of free α-glucosidase (E) and α-glucosidase complexes with MD-IPMP (F), MVD-IPMP (G), IRD-IPMP (H), and HD-IPMP (I) derived from FT-IR spectra in the range of 1700–1600 cm^{-1}; Schematic diagram illustrating the effect of IPMPs on the secondary structure of α-glucosidase (J).

UV spectroscopy findings corroborate the previously mentioned fluorescence data, providing further evidence that the four IPMPs can induce structural alterations in α-glucosidase at specific binding sites.

FT-IR offers valuable insights into protein secondary structures, as the amide bands correspond to distinct peptide vibrations. These amide groups are sensitive to structural changes (Tang et al., 2019). Notably, the amide I band (1700–1600 cm^{-1}) and II band (1600–1500 cm^{-1}), corresponding to C═O stretching, C − N stretching and N − H bending, are crucial for analyzing protein structure (Zhang et al., 2012). To investigate how IPMPs influence α-glucosidase's secondary structure, FT-IR spectra of the amide I band were analyzed in the presence of IPMPs using techniques such as self-deconvolution, second-order derivative enhancement, and curve fitting (Wang et al., 2016). As shown in Fig. 6E–I, the addition of IPMPs caused the amide I band peak to shift from 1650 cm^{-1} to 1653 cm^{-1} (MD-IPMP), 1657 cm^{-1} (MVD-IPMP), 1654 cm^{-1} (HD-IPMP), and 1655 cm^{-1} (IRD-IPMP). These shifts suggest that IPMPs interact with the C═O groups in α-glucosidase, inducing rearrangements in the hydrogen bonding network of the protein (Abudurexiti et al., 2024).

Protein secondary structures in the amide I band are categorized as β-sheets (1615–1637 cm^{-1}), random coils (1638–1648 cm^{-1}), α-helices (1649–1660 cm^{-1}), β-turns (1661–1680 cm^{-1}), and β-antiparallel structures (1681–1692 cm^{-1}) (Zhang et al., 2012). To explore how IPMPs affect the enzyme's secondary structure, the percentage of each structural component was calculated based on the integral areas, as summarized in Table 2b. In free α-glucosidase, the structure consisted of 30.59 % α-helix, 28.61 % β-sheet, 12.81 % β-turn, 15.85 % random coil, and 12.14 % β-antiparallel. After adding MD-IPMP, MVD-IPMP, IRD-IPMP, and HD-IPMP, the α-helix content significantly decreased to 16.05 %, 13.34 %, 21.33 %, and 18.82 %, respectively. The β-sheet content rose to 31.23 % with MD-IPMP and 40.72 % with MVD-IPMP, while it decreased to 20.85 % with IRD-IPMP and 27.67 % with HD-IPMP. The random coil and β-antiparallel contents also showed variations: MD-IPMP, IRD-IPMP, and HD-IPMP increased to 17.49 %, 22.22 %, and 18.92 %, and 12.86 %, 16.81 %, and 13.97 %, respectively. However, MVD-IPMP-α-glucosidase showed a decrease in random coil and β-antiparallel content to 13.74 % and 9.50 %, respectively. These shifts suggest that the inhibitors are influencing the enzyme's secondary structure. The decrease in α-helix content alongside an increase in disordered structures indicates that inhibitor binding could lead to protein unfolding (Wang et al., 2018). The rise in β-sheet and β-turn content indicates that the inhibitors modify the polypeptide structure, resulting in the closure of the enzyme's active site, diminished substrate binding, and reduced enzyme activity (Wang et al., 2020). In conclusion, IPMPs bind to α-glucosidase, inducing changes in its polarity and molecular conformation. These alterations affect the enzyme's ability to bind substrates and may prevent the formation of the active site, leading to enzyme inhibition. The proposed mechanism by which IPMPs inhibit α-glucosidase is illustrated in Fig. 6J (By Figdraw), showing how polysaccharide binding induces conformational changes and disrupts the hydrogen bonding network that maintains the enzyme's secondary structure. The distinct impacts of the four IPMPs on each secondary structure component are likely attributed to variations in their polysaccharide structures, which arise from different drying methods. Notably, MVD-IPMP had the most significant effect on all five secondary structure components of α-glucosidase, which aligns with its strong inhibitory activity. The combined insights from FT-IR and UV spectroscopy deepen our understanding of how IPMPs inhibit α-glucosidase by affecting substrate binding and enzyme inactivation.

Table 2b
Content of different secondary structures of free α-glucosidase and α-glucosidase-IPMP complexes (FT-IR spectroscopy).

Sample	α-Helix (%)	β-Sheet (%)	β-Turn (%)	Random coil (%)	β-Antiparallel (%)
α-Glucosidase	30.59	28.61	12.81	15.85	12.14
α-Glucosidase + MD-IPMP	16.05	31.23	22.38	17.49	12.86
α-Glucosidase + MVD-IPMP	13.34	40.72	22.70	13.74	9.50
α-Glucosidase + IRD-IPMP	21.33	20.85	18.79	22.22	16.81
α-Glucosidase + HD-IPMP	18.82	27.67	20.62	18.92	13.97

4. Conclusion

This study examined how various drying methods influence the physicochemical properties, structural features, and in vitro biological activities—such as antioxidant, antiglycation, and α-glucosidase inhibition—of IPMPs. The results demonstrated that the drying method significantly influenced both the physicochemical properties and biological activities of IPMPs. Drying methods affected key quality attributes, including extraction yield, total sugar content, uronic acid levels, monosaccharide composition, molecular weight distribution, thermal stability, chain conformation, and microstructure. Among the different drying techniques, MVD resulted in IPMP with lower molecular weight, higher uronic acid content, and a distinctive triple-helix structure. These traits enhanced the MVD-IPMP' ability to inhibit linoleic acid oxidation, glycation, and α-glucosidase activity in vitro. All IPMPs inhibited α-glucosidase through a combined mechanism, predominantly via static quenching, which led to reduced fluorescence, with MVD-IPMP exhibiting the highest binding affinity. Both fluorescence and FT-IR infrared spectroscopy confirmed that IPMPs interact with α-glucosidase, causing alterations in its secondary structure. The results indicate that MVD is an effective method for extracting bioactive polysaccharides from IPM cake meal, with enhanced antioxidant, antiglycation, and hypoglycemic activities. These findings may provide a theoretical foundation for the use of MVD-IPMP as a natural antioxidant and hypoglycemic agent in functional foods and pharmaceutical applications. In conclusion, this study provides strong evidence supporting microwave vacuum drying for the industrial extraction and processing of high-quality polysaccharides from IPM cake meal. While most research on dried polysaccharides' bioactivities is conducted in vitro, future studies should explore their in vivo effects. Further purification and detailed structural analyses are essential to enhance understanding of the structure-bioactivity relationship in IPMPs.

CRediT authorship contribution statement

Qiuqiu Zhang: Writing – original draft, Validation, Formal analysis, Data curation. **Renshuai Huang:** Writing – review & editing, Formal analysis. **Lisha Wang:** Writing – review & editing. **Yonghui Ge:** Formal analysis. **Honggang Fang:** Formal analysis. **Guangjing Chen:** Writing – review & editing, Visualization, Supervision, Funding acquisition, Conceptualization.

Declaration of competing interest

The authors declare that they have no known competing financial interests or personal relationships that could have appeared to influence the work reported in this paper.

Acknowledgement

This work was supported by Special Fund Project of Guizhou Forestry Bureau (No. GZ-LFGS-HZ-135-011), Guizhou Provincial Major Scientific and Technological Program (No. [2024]025), Guizhou Province High Level Innovative Talent Training Program - "1000" talents (No. ZKHT-GCC-[2023]001), and Graduate Student Scientific Research Innovation Project of Guiyang University (2023-YJS02).

Appendix A. Supplementary data

Supplementary data to this article can be found online at https://doi.org/10.1016/j.fochx.2025.102348.

Data availability

Data will be made available on request.

References

Abudurexiti, A., Abdurahman, A., Zhang, R., Zhong, Y., Lei, Y., Qi, S., Hou, W., & Ma, X. (2024). Screening of α-glucosidase inhibitors in *Cichorium glandulosum* Boiss. Et Huet extracts and study of interaction mechanisms. *Acs. Omega, 9*(17), 19401–19417. https://doi.org/10.1021/acsomega.4c00699

Amamou, S., Lazreg, H., Hafsa, J., Majdoub, H., Rihouey, C., Le Cerf, D., & Achour, L. (2020). Effect of extraction condition on the antioxidant, antiglycation and α-amylase inhibitory activities of *Opuntia macrorhiza* fruit peels polysaccharides. *Lwt-Food Science and Technology, 127*, Article 109411. https://doi.org/10.1016/j.lwt.2020.109411

An, K. J., Wu, J. J., Xiao, H. W., Hu, T. G., Yu, Y. S., Yang, W. Y., … Xu, Y. J. (2022). Effect of various drying methods on the physicochemical characterizations, antioxidant activities and hypoglycemic activities of lychee (*Litchi chinensis* Sonn.) pulp polysaccharides. *International Journal of Biological Macromolecules, 220*, 510–519. https://doi.org/10.1016/j.ijbiomac.2022.08.083

Babbar, N., Van Roy, S., Wijnants, M., Dejonghe, W., Caligiani, A., Sforza, S., & Elst, K. (2016). Effect of extraction conditions on the saccharide (neutral and acidic) composition of the crude Pectic extract from various agro-industrial residues. *Journal of Agricultural and Food Chemistry, 64*(1), 268–276. https://doi.org/10.1021/acs.jafc.5b04394

Bhuiyan, M. N. I., Mitsuhashi, S., Sigetomi, K., & Ubukata, M. (2017). Quercetin inhibits advanced glycation end product formation via chelating metal ions, trapping methylglyoxal, and trapping reactive oxygen species. *Bioscience Biotechnology and Biochemistry, 81*(5), 882–890. https://doi.org/10.1080/09168451.2017.1282805

Blumenkr, N., & Asboehan, G. (1973). New method for quantitative-determination of uronic acids. *Analytical Biochemistry, 54*(2), 484–489. https://doi.org/10.1016/0003-2697(73)90377-1

Chaouch, M. A., Hafsa, J., Rihouey, C., Le Cerf, D., & Majdoub, H. (2015). Depolymerization of polysaccharides from Opuntia ficus indica: Antioxidant and antiglycated activities. *International Journal of Biological Macromolecules, 79*, 779–786. https://doi.org/10.1016/j.ijbiomac.2015.06.003

Chen, G., Fang, C., Ran, C., Tan, Y., Yu, Q., & Kan, J. (2019). Comparison of different extraction methods for polysaccharides from bamboo shoots (*Chimonobambusa quadrangularis*) processing by-products. *International Journal of Biological Macromolecules, 130*, 903–914. https://doi.org/10.1016/j.ijbiomac.2019.03.038

Chen, G., Li, C., Wang, S., Mei, X., Zhang, H., & Kan, J. (2019a). Characterization of physicochemical properties and antioxidant activity of polysaccharides from shoot residues of bamboo (*Chimonobambusa quadrangularis*): Effect of drying procedures. *Food Chemistry, 292*, 281–293. https://doi.org/10.1016/j.foodchem.2019.04.060

Chen, G., Sun, J., Dai, Q., Sun, M., & Hu, P. (2024). Polysaccharides from seedless chestnut rose (*Rosa sterilis*) fruits: Insights into innovative drying technologies and their structural characteristics, antioxidant, Antiglycation, and α-glucosidase inhibitory activities. *Foods, 13*(16), 2483. https://doi.org/10.3390/foods13162483

Chen, G., Sun, M., Chen, K., Wang, L., & Sun, J. (2024). Ultrasonic-assisted Decoloration of polysaccharides from seedless chestnut rose (*Rosa sterilis*) fruit: Insight into the impact of different macroporous resins on its structural characterization and in vitro hypoglycemic activity. *Foods, 13*(9), 1349. https://doi.org/10.3390/foods13091349

Chen, G. J., Hong, Q. Y., Ji, N., Wu, W. N., & Ma, L. Z. (2020). Influences of different drying methods on the structural characteristics and prebiotic activity of polysaccharides from bamboo shoot (*Chimonobambusa quadrangularis*) residues. *International Journal of Biological Macromolecules, 155*, 674–684. https://doi.org/10.1016/j.ijbiomac.2020.03.223

Chen, K., Zhang, Q., Yang, S., Zhang, S., & Chen, G. (2024). Comparative study on the impact of different extraction technologies on structural characteristics, physicochemical properties, and biological activities of polysaccharides from seedless chestnut rose (Rosa sterilis) fruit. *Foods, 13*(5), 772. https://doi.org/10.3390/foods13050772

Chen, S., Qin, L., Xie, L. M., Yu, Q., Chen, Y., Chen, T., … Xie, J. H. (2022). Physicochemical characterization, rheological and antioxidant properties of three alkali-extracted polysaccharides from mung bean skin. *Food Hydrocolloids, 132*, Article 107867. https://doi.org/10.1016/j.foodhyd.2022.107867

Deng, Z. D., Pan, Y. G., Chen, W. X., Chen, W. J., Yun, Y. H., Zhong, Q. P., … Chen, H. M. (2020). Effects of cultivar and growth region on the structural, emulsifying and rheological characteristic of mango peel pectin. *Food Hydrocolloids, 103*, Article 105707. https://doi.org/10.1016/j.foodhyd.2020.105707

Dong, H., Dai, T., Liang, L., Deng, L., Liu, C., Li, Q., Liang, R., & Chen, J. (2021). Physicochemical properties of pectin extracted from navel orange peel dried by vacuum microwave. *Lwt-Food Science and Technology, 151*, Article 112100. https://doi.org/10.1016/j.lwt.2021.112100

Dong, Y.-H., Wang, Z.-X., Chen, C., Wang, P.-P., & Fu, X. (2023). A review on the hypoglycemic effect, mechanism and application development of natural dietary polysaccharides. *International Journal of Biological Macromolecules, 253*, Article 127267. https://doi.org/10.1016/j.ijbiomac.2023.127267

van Dongen, K. C. W., Linkens, A. M. A., Wetzels, S. M. W., Wouters, K., Vanmierlo, T., van de Waarenburg, M. P. H., … Schalkwijk, C. G. (2021). Dietary advanced glycation endproducts (AGEs) increase their concentration in plasma and tissues, result in inflammation and modulate gut microbial composition in mice; evidence for reversibility. *Food Research International, 147*, 110547. https://doi.org/10.1016/j.foodres.2021.110547

Dou, L., Zhang, Z., Yang, W., Chen, Y., Luo, K., & Kan, J. (2024). Separation and purification of antioxidant peptides from *Idesia polycarpa* maxim. Cake meal and study of conformational relationship between them. *Food Science & Nutrition, 12*(9), 6206–6225. https://doi.org/10.1002/fsn3.4325

Dou, Z., Chen, C., & Fu, X. (2019). The effect of ultrasound irradiation on the physicochemical properties and α-glucosidase inhibitory effect of blackberry fruit polysaccharide. *Food Hydrocolloids, 96*, 568–576. https://doi.org/10.1016/j.foodhyd.2019.06.002

Dou, Z. M., Chen, C., Huang, Q., & Fu, X. (2021). Comparative study on the effect of extraction solvent on the physicochemical properties and bioactivity of blackberry fruit polysaccharides. *International Journal of Biological Macromolecules, 183*, 1548–1559. https://doi.org/10.1016/j.ijbiomac.2021.05.131

Dubois, M., Gilles, K. A., Hamilton, J. K., Rebers, P. A., & Smith, F. (1956). Colorimetic method for determination of sugars and related substances. *Analytical Chemistry, 28*(3), 350–356. https://doi.org/10.1021/ac60111a017

Fei, Q., Gao, Y., Zhang, X., Sun, Y., Hu, B., Zhou, L., Jabbar, S., & Zeng, X. (2014). Effects of oolong tea polyphenols, EGCG, and EGCG3 me on pancreatic α-amylase activity in vitro. *Journal of Agricultural and Food Chemistry, 62*(39), 9507–9514. https://doi.org/10.1021/jf5032907

Fu, Y., Feng, K. L., Wei, S. Y., Xiang, X. R., Ding, Y., Li, H. Y., … Wu, D. T. (2020). Comparison of structural characteristics and bioactivities of polysaccharides from loquat leaves prepared by different drying techniques. *International Journal of Biological Macromolecules, 145*, 611–619. https://doi.org/10.1016/j.ijbiomac.2019.12.226

Gavahian, M., Mathad, G. N., Pandiselvam, R., Lin, J., & Sun, D.-W. (2021). Emerging technologies to obtain pectin from food processing by-products: A strategy for enhancing resource efficiency. *Trends in Food Science & Technology, 115*, 42–54. https://doi.org/10.1016/j.tifs.2021.06.018

Guo, D. Q., Yin, X. X., Wu, D. M., Chen, J. L., & Ye, X. Q. (2023). Natural polysaccharides from Glycyrrhiza uralensis residues with typical glucan structure showing inhibition on α-glucosidase activities. *International Journal of Biological Macromolecules, 224*, 776–785. https://doi.org/10.1016/j.ijbiomac.2022.10.165

Guo, H., Liu, H.-Y., Li, H., Wu, D.-T., Zhong, L. L. D., Gan, R.-Y., & Gao, H. (2023). Recent advances in the influences of drying technologies on physicochemical properties and biological activities of plant polysaccharides. *Critical Reviews in Food Science and Nutrition, 64*(33), 13024–13044. https://doi.org/10.1080/10408398.2023.2259983

Hou, K., Yang, X., Bao, M., Chen, F., Tian, H., & Yang, L. (2018). Composition, characteristics and antioxidant activities of fruit oils from Idesia polycarpa using homogenate-circulating ultrasound-assisted aqueous enzymatic extraction. *Industrial Crops and Products, 117*, 205–215. https://doi.org/10.1016/j.indcrop.2018.03.001

Ji, X., Guo, J., Cao, T., Zhang, T., Liu, Y., & Yan, Y. (2023). Review on mechanisms and structure-activity relationship of hypoglycemic effects of polysaccharides from natural resources. *Food Science and Human Wellness, 12*(6), 1969–1980. https://doi.org/10.1016/j.fshw.2023.03.017

Jia, Y. N., Gao, X. D., Xue, Z. H., Wang, Y. J., Lu, Y. P., Zhang, M., … Chen, H. X. (2020). Characterization, antioxidant activities, and inhibition on a-glucosidase activity of corn silk polysaccharides obtained by different extraction methods. *International Journal of Biological Macromolecules, 163*, 1640–1648. https://doi.org/10.1016/j.ijbiomac.2020.09.068

Jia, Y. N., Xue, Z. H., Wang, Y. J., Lu, Y. P., Li, R. L., Li, N. N., … Chen, H. X. (2021). Chemical structure and inhibition on α-glucosidase of polysaccharides from corn silk by fractional precipitation. *Carbohydrate Polymers, 252*, Article 117185. https://doi.org/10.1016/j.carbpol.2020.117185

Jin, M.-Y., Li, M.-Y., Huang, R.-M., Wu, X.-Y., Sun, Y.-M., & Xu, Z.-L. (2021). Structural features and anti-inflammatory properties of pectic polysaccharides: A review. *Trends in Food Science & Technology, 107*, 284–298. https://doi.org/10.1016/j.tifs.2020.10.042

Katz, C., Cohen-Or, I., Gophna, U., & Ron, E. Z. (2010). The ubiquitous conserved Glycopeptidase Gcp prevents accumulation of toxic glycated proteins. *Mbio, 1*(3), e00195–e00210. https://doi.org/10.1128/mBio.00195-10

Kubbutat, P., Kulozik, U., & Dombrowski, J. (2021). Foam structure preservation during microwave-assisted vacuum drying: Significance of interfacial and dielectric properties of the bulk phase of foams from Polysorbate 80-maltodextrin dispersions. *Foods, 10*(6), 1163. https://doi.org/10.3390/foods10061163

Li, F., Feng, K. L., Yang, J. C., He, Y. S., Guo, H., Wang, S. P., … Wu, D. T. (2021). Polysaccharides from dandelion (*Taraxacum mongolicum*) leaves: Insights into innovative drying techniques on their structural characteristics and biological activities. *International Journal of Biological Macromolecules, 167*, 995–1005. https://doi.org/10.1016/j.ijbiomac.2020.11.054

Li, N., Sun, Y.-R., He, L.-B., Huang, L., Li, T.-T., Wang, T.-Y., Tang, L., & Tang, L. (2020). *Amelioration by Idesia polycarpa Maxim. Var. vestita Diels. Of oleic acid-induced nonalcoholic fatty liver in HepG2 cells through antioxidant and modulation of lipid metabolism. Oxidative medicine and cellular longevity, 2020, 1208726*. https://doi.org/10.1155/2020/1208726

Li, Q. Y., Dou, Z. M., Duan, Q. F., Chen, C., Liu, R. H., Jiang, Y. M., … Fu, X. (2024). A comparison study on structure-function relationship of polysaccharides obtained from sea buckthorn berries using different methods: Antioxidant and bile acid-binding capacity. *Food Science and Human Wellness, 13*(1), 494–505. https://doi.org/10.26599/fshw.2022.9250043

Li, Y., Peng, T., Huang, L., Zhang, S. Y., He, Y. Y., & Tang, L. (2019). The evaluation of lipids raw material resources with the fatty acid profile and morphological characteristics of *Idesia polycarpa* Maxim. Var. vestita Diels fruit in harvesting. *Industrial Crops and Products, 129*, 114–122. https://doi.org/10.1016/j.indcrop.2018.11.071

Li, Z., Zhou, B., Zheng, T., Zhao, C., Gao, Y., Wu, W., Fan, Y., Wang, X., Qiu, M., & Fan, J. (2023). Structural characteristics, rheological properties, and antioxidant and anti-glycosylation activities of pectin polysaccharides from Arabica coffee husks. *Foods, 12*(2), 423. https://doi.org/10.3390/foods12020423

Liu, W., Li, F., Wang, P., Liu, X., He, J.-J., Xian, M.-L., Zhao, L., Qin, W., Gan, R.-Y., & Wu, D.-T. (2020). Effects of drying methods on the physicochemical characteristics and bioactivities of polyphenolic-protein-polysaccharide conjugates from Hovenia dulcis. *International Journal of Biological Macromolecules, 148*, 1211–1221. https://doi.org/10.1016/j.ijbiomac.2019.10.211

Luo, T., Xu, J., Zhen, Z., Pan, X., Feng, L., Qin, L., & Ren, T. (2025). Quality analysis of Idesia polycarpa fruit oil samples from cultivars with different phenotypes. *Food Chemistry: X, 25*, Article 102127. https://doi.org/10.1016/j.fochx.2024.102127

Ma, L., He, Q., Qiu, Y., Liu, H., Wu, J., Liu, G., … Zhu, L. (2021). Food matrixes play a key role in the distribution of contaminants of lipid origin: A case study of malondialdehyde formation in vegetable oils during deep-frying. *Food Chemistry, 347*, Article 129080. https://doi.org/10.1016/j.foodchem.2021.129080

Mannai, F., Elhleli, H., Yilmaz, M., Khiari, R., Belgacem, M. N., & Moussaoui, Y. (2023). Precipitation solvents effect on the extraction of mucilaginous polysaccharides from *Opuntia ficus-indica* (Cactaceae): Structural, functional and rheological properties. *Industrial Crops and Products, 202*, Article 117072. https://doi.org/10.1016/j.indcrop.2023.117072

Meng, Q. R., Chen, F., Xiao, T. C., & Zhang, L. F. (2019). Inhibitory effects of polysaccharide from *Diaphragma juglandis fructus* on α-amylase and α-D-glucosidase activity, streptozotocin-induced hyperglycemia model, advanced glycation end-products formation, and H_2O_2-induced oxidative damage. *International Journal of Biological Macromolecules, 124*, 1080–1089. https://doi.org/10.1016/j.ijbiomac.2018.12.011

Menon, A., Stojceska, V., & Tassou, S. A. (2020). A systematic review on the recent advances of the energy efficiency improvements in non-conventional food drying technologies. *Trends in Food Science & Technology, 100*, 67–76. https://doi.org/10.1016/j.tifs.2020.03.014

Mohammed, A. S. A., Naveed, M., & Jost, N. (2021). Polysaccharides; classification, chemical properties, and future perspective applications in fields of pharmacology and biological medicine (a review of current applications and upcoming potentialities). *Journal of Polymers and the Environment, 29*(8), 2359–2371. https://doi.org/10.1007/s10924-021-02052-2

Mohammed, J. K., Mahdi, A. A., Ahmed, M. I., Ma, M. J., & Wang, H. X. (2020). Preparation, deproteinization, characterization, and antioxidant activity of polysaccharide from *Medemia Argun* fruit. *International Journal of Biological Macromolecules, 155*, 919–926. https://doi.org/10.1016/j.ijbiomac.2019.11.050

Munir, H., Shahid, M., Anjum, F., & Mudgil, D. (2016). Structural, thermal and rheological characterization of modified Dalbergia sissoo gum—A medicinal gum. *International Journal of Biological Macromolecules, 84*, 236–245. https://doi.org/10.1016/j.ijbiomac.2015.12.001

Rotariu, D., Babes, E. E., Tit, D. M., Moisi, M., Bustea, C., Stoicescu, M., … Bungau, S. G. (2022). Oxidative stress - complex pathological issues concerning the hallmark of cardiovascular and metabolic disorders. *Biomedicine & Pharmacotherapy, 152*, Article 113238. https://doi.org/10.1016/j.biopha.2022.113238

Sevag, M. G., Lackman, D. B., & Smolens, J. (1938). The isolation of the components of streptococcal nucleoproteins in serologically active form. *Journal of Biological Chemistry, 124*(2), 0425–0436. https://doi.org/10.1016/S0021-9258(18)74048-9

Shi, X., Zhang, Q., Yang, J., Huang, R., Ge, Y., Wang, J., & Chen, G. (2024). Simultaneous extraction of oil, protein and polysaccharide from *Idesia polycarpa* maxim cake meal using ultrasound combined with three phase partitioning. *Ultrasonics Sonochemistry, 110*, Article 107043. https://doi.org/10.1016/j.ultsonch.2024.107043

Shi, X., Zhang, X., Wang, L., Ge, Y., & Chen, G. (2025). Comparative study of Idesia polycarpa maxim cake meal polysaccharides: Conventional versus innovative extraction methods and their impact on structural features, emulsifying, antiglycation, and hypoglycemic properties. *Food Chemistry, 471*, Article 142745. https://doi.org/10.1016/j.foodchem.2024.142745

Shiyu, Z., Bo, W., Weiqiao, L., Bingzheng, L., Hongwei, X., & Rongru, L. (2024). Physicochemical properties, structure and biological activity of ginger polysaccharide: Effect of microwave infrared dual-field coupled drying. *International Journal of Biological Macromolecules, 281*(Part 3), 136474. https://doi.org/10.1016/j.ijbiomac.2024.136474

Spínola, V., Llorent-Martínez, E. J., & Castilho, P. C. (2020). Inhibition of α-amylase, α-glucosidase and pancreatic lipase by phenolic compounds of *Rumex maderensis* (Madeira sorrel). Influence of simulated gastrointestinal digestion on hyperglycaemia-related damage linked with aldose reductase activity and protein glycation. *Lwt-food. Science and Technology, 118*, Article 108727. https://doi.org/10.1016/j.lwt.2019.108727

Su, C.-H., Lai, M.-N., & Ng, L.-T. (2017). Effects of different extraction temperatures on the physicochemical properties of bioactive polysaccharides from *Grifola frondosa*. *Food Chemistry, 220*, 400–405. https://doi.org/10.1016/j.foodchem.2016.09.181

Tan, M. H., Zhao, Q. S., & Zhao, B. (2021). Physicochemical properties, structural characterization and biological activities of polysaccharides from quinoa (Chenopodium quinoa Willd.) seeds. *International Journal of Biological Macromolecules, 193*, 1635–1644. https://doi.org/10.1016/j.ijbiomac.2021.10.226

Tang, H., Ma, F., Zhao, D., & Xue, Z. (2019). Exploring the effect of salvianolic acid C on α-glucosidase: Inhibition kinetics, interaction mechanism and molecular modelling methods. *Process Biochemistry, 78*, 178–188. https://doi.org/10.1016/j.procbio.2019.01.011

Tang, X., Zhang, Y., Li, F., Zhang, N., Yin, X., Zhang, B., Zhang, B., Ni, W., Wang, M., & Fan, J. (2023). Effects of traditional and advanced drying techniques on the physicochemical properties of *Lycium barbarum* L. polysaccharides and the formation of Maillard reaction in its dried berries. *Food Chemistry, 409*, 135268. https://doi.org/10.1016/j.foodchem.2022.135268

Tian, B., Zhao, Q., Xing, H., Xu, J., Li, Z., Zhu, H., Yang, K., Sun, P., & Cai, M. (2022). Gastroprotective effects of *Ganoderma lucidum* polysaccharides with different molecular weights on ethanol-induced acute gastric injury in rats. *Nutrients, 14*(7), 1476. https://doi.org/10.3390/nu14071476

Tian, Y., Zhao, Y., Huang, J., Zeng, H., & Zheng, B. (2016). Effects of different drying methods on the product quality and volatile compounds of whole shiitake mushrooms. *Food Chemistry, 197*, 714–722. https://doi.org/10.1016/j.foodchem.2015.11.029

Wan, X., Wang, J., Zhang, S., Zhang, X., Shi, X., & Chen, G. (2025). New insights into adlay seed bran polysaccharides: Effects of enzyme-assisted aspergillus Niger solid-state fermentation on its structural features, simulated gastrointestinal digestion, and prebiotic activity. *International Journal of Biological Macromolecules, 284*(P1), 138101. https://doi.org/10.1016/j.ijbiomac.2024.138101

Wang, L., Chen, C., Zhang, B., Huang, Q., Fu, X., & Li, C. (2018). Structural characterization of a novel acidic polysaccharide from Rosa roxburghii Tratt fruit and its α-glucosidase inhibitory activity. *Food & Function, 9*(7), 3974–3985. https://doi.org/10.1039/c8fo00561c

Wang, N., Chen, Z., Lv, J., Li, T., Wu, H., Wu, J., Wu, H., & Xiang, W. (2023). Characterization, hypoglycemia and antioxidant activities of polysaccharides from Rhodosorus sp. SCSIO-45730. *Industrial Crops and Products, 191*, Article 115936. https://doi.org/10.1016/j.indcrop.2022.115936

Wang, Q., Huang, C.-R., Jiang, M., Zhu, Y.-Y., Wang, J., Chen, J., & Shi, J.-H. (2016). Binding interaction of atorvastatin with bovine serum albumin: Spectroscopic methods and molecular docking. *Spectrochimica Acta Part a-Molecular and Biomolecular Spectroscopy, 156*, 155–163. https://doi.org/10.1016/j.saa.2015.12.003

Wang, S., Xie, X., Zhang, L., Hu, Y.-M., Wang, H., & Tu, Z.-C. (2020). Inhibition mechanism of α-glucosidase inhibitors screened from Artemisia selengensis Turcz root. *Industrial Crops and Products, 143*, 111941. https://doi.org/10.1016/j.indcrop.2019.111941

Wang, Y., Li, X., Zhao, P., Qu, Z., Bai, D. T., Gao, X. X., … Gao, W. Y. (2019). Physicochemical characterizations of polysaccharides from Angelica Sinensis Radix under different drying methods for various applications. *International Journal of Biological Macromolecules, 121*, 381–389. https://doi.org/10.1016/j.ijbiomac.2018.10.035

Wen, L. Y., Xiang, X. W., Wang, Z. R., Yang, Q. Q., Guo, Z. H., Huang, P. M., … Kan, J. Q. (2022). Evaluation of cultivars diversity and lipid composition properties of *Idesia polycarpa var. vestita* Diels. *Journal of Food Science, 87*(9), 3841–3855. https://doi.org/10.1111/1750-3841.16293

Wu, B. G., Qiu, C. C., Guo, Y. T., Zhang, C. H., Li, D., Gao, K., … Ma, H. L. (2022). Comparative evaluation of physicochemical properties, microstructure, and antioxidant activity of jujube polysaccharides subjected to hot air, infrared, radio frequency, and freeze drying. *Agriculture-Basel, 12*(10), 1606. https://doi.org/10.3390/agriculture12101606

Xiang, X. W., Wen, L. Y., Wang, Z. R., Yang, G., Mao, J. M., An, X. F., & Kan, J. Q. (2023). A comprehensive study on physicochemical properties, bioactive compounds, and emulsified lipid digestion characteristics of *Idesia polycarpa var. Vestita Diels fruits oil. Food Chemistry, 404*, Article 134634. https://doi.org/10.1016/j.foodchem.2022.134634

Xiong, F., Li, X., Zheng, L. H., Hu, N., Cui, M. J., & Li, H. Y. (2019). Characterization and antioxidant activities of polysaccharides from Passiflora edulis Sims peel under different degradation methods. *Carbohydrate Polymers, 218*, 46–52. https://doi.org/10.1016/j.carbpol.2019.04.069

Xiong, G. Y., Ma, L. S., Zhang, H., Li, Y. P., Zou, W. S., Wang, X. F., … Wang, X. Y. (2022). Physicochemical properties, antioxidant activities and α-glucosidase inhibitory effects of polysaccharides from *Evodiae fructus* extracted by different solvents. *International Journal of Biological Macromolecules, 194*, 484–498. https://doi.org/10.1016/j.ijbiomac.2021.11.092

Xue, H., Hao, Z., Gao, Y., Cai, X., Tang, J., Liao, X., & Tan, J. (2023). Research progress on the hypoglycemic activity and mechanisms of natural polysaccharides. *International Journal of Biological Macromolecules, 252*, 126199. https://doi.org/10.1016/j.ijbiomac.2023.126199

Yan, J. K., Wu, L. X., Qiao, Z. R., Cai, W. D., & Ma, H. L. (2019). Effect of different drying methods on the product quality and bioactive polysaccharides of bitter gourd (*Momordica charantia* L.) slices. *Food Chemistry, 271*, 588–596. https://doi.org/10.1016/j.foodchem.2018.08.012

Yang, B., Luo, Y., Sang, Y., & Kan, J. (2022). Isolation, purification, structural characterization, and hypoglycemic activity assessment of polysaccharides from *Hovenia dulcis* (Guai Zao). *International Journal of Biological Macromolecules, 208*, 1106–1115. https://doi.org/10.1016/j.ijbiomac.2022.03.211

Yang, B., Luo, Y., Wei, X., & Kan, J. (2022). Polysaccharide from *Hovenia dulcis* (Guaizao) improves pancreatic injury and regulates liver glycometabolism to alleviate STZ-induced type 1 diabetes mellitus in rats. *International Journal of Biological Macromolecules, 214*, 655–663. https://doi.org/10.1016/j.ijbiomac.2022.06.147

Yang, M.-H., Yang, Y., Zhou, X., & Chen, H.-G. (2024). Advances in polysaccharides of natural source of anti-diabetes effect and mechanism. *Molecular Biology Reports, 51*(1), 101. https://doi.org/10.1007/s11033-023-09081-1

Yang, W., Zhang, Z., Chen, Y., & Luo, K. (2023). Evaluation of the use of *Idesia polycarpa* maxim protein coating to extend the shelf life of European sweet cherries. *Frontiers in Nutrition, 10*, 1283086. https://doi.org/10.3389/fnut.2023.1283086

Ye, K., Fu, C., Ma, S., Du, H., Chen, S., Liu, D., Ma, G., & Xiao, H. (2023). Comprehensive assessment of *Hypsizygus marmoreus* polysaccharides through simulated digestion and gut microbiota fermentation *in vitro*. *Food Hydrocolloids, 144*, Article 108989. https://doi.org/10.1016/j.foodhyd.2023.108989

Yi, Y., Xu, W., Wang, H.-X., Huang, F., & Wang, L.-M. (2020). Natural polysaccharides experience physiochemical and functional changes during preparation: A review. *Carbohydrate Polymers, 234*, Article 115896. https://doi.org/10.1016/j.carbpol.2020.115896

Yu, G., Zhang, Q., Wang, Y., Yang, Q., Yu, H., Li, H., Chen, J., & Fu, L. (2021). Sulfated polysaccharides from red seaweed Gelidium amansii: Structural characteristics, antioxidant and anti-glycation properties, and development of bioactive films. *Food Hydrocolloids, 119*, Article 106820. https://doi.org/10.1016/j.foodhyd.2021.106820

Yu, Y., Shen, M., Song, Q., & Xie, J. (2018). Biological activities and pharmaceutical applications of polysaccharide from natural resources: A review. *Carbohydrate Polymers, 183*, 91–101. https://doi.org/10.1016/j.carbpol.2017.12.009

Yuan, Q., He, Y., Xiang, P. Y., Huang, Y. J., Cao, Z. W., Shen, S. W., … Wu, D. T. (2020). Influences of different drying methods on the structural characteristics and multiple bioactivities of polysaccharides from okra (*Abelmoschus esculentus*). *International Journal of Biological Macromolecules, 147*, 1053–1063. https://doi.org/10.1016/j.ijbiomac.2019.10.073

Zartha Sossa, J. W., Orozco, G. L., García Murillo, L. M., Peña Osorio, M., & Sánchez Suarez, N. (2021). Infrared drying trends applied to fruit. *Frontiers in Sustainable Food Systems, 5*, Article 650690. https://doi.org/10.3389/fsufs.2021.650690

Zeng, L., Ding, H. F., Hu, X., Zhang, G. W., & Gong, D. M. (2019). Galangin inhibits α-glucosidase activity and formation of non-enzymatic glycation products. *Food Chemistry, 271*, 70–79. https://doi.org/10.1016/j.foodchem.2018.07.148

Zeng, L., Zhang, G., Liao, Y., & Gong, D. (2016). Inhibitory mechanism of morin on α-glucosidase and its anti-glycation properties. *Food & Function, 7*(9), 3953–3963. https://doi.org/10.1039/c6fo00680a

Zeng, S., Wang, B., Lv, W., Li, B., Xiao, H., & Lin, R. (2024). Physicochemical properties, structure and biological activity of ginger polysaccharide: Effect of microwave infrared dual-field coupled drying. *International Journal of Biological Macromolecules, 281*(P3), Article 136474. https://doi.org/10.1016/j.ijbiomac.2024.136474

Zhang, G., Wang, L., & Pan, J. (2012). Probing the binding of the flavonoid Diosmetin to human serum albumin by multispectroscopic techniques. *Journal of Agricultural and Food Chemistry, 60*(10), 2721–2729. https://doi.org/10.1021/jf205260g

Zhang, Q., Wu, S., Dai, Q., Hu, P., & Chen, G. (2024). Effects of different drying methods on the structural characteristics and multiple bioactivities of *Rosa roxburghii* Tratt fruit polysaccharides. *Foods, 13*(15), 2417. https://doi.org/10.3390/foods13152417

Zhang, Y., Pan, Y., Li, J., Zhang, Z., He, Y., Yang, H., & Zhou, P. (2022). Inhibition on α-glucosidase activity and non-enzymatic glycation by an anti-oxidative proteoglycan from *Ganoderma lucidum*. *Molecules, 27*(5), 1457. https://doi.org/10.3390/molecules27051457

Zhao, M., Wu, Y., Zhang, F., Zheng, S., Wang, L., Bai, J., & Yang, Y. (2023). Preparation of *Ribes nigrum* L. polysaccharides-stabilized selenium nanoparticles for enhancement of the anti-glycation and α-glucosidase inhibitory activities. *International Journal of Biological Macromolecules, 253*(P5), 127122. https://doi.org/10.1016/j.ijbiomac.2023.127122

Zhao, M. M., Bai, J. W., Bu, X. Y., Yin, Y. T., Wang, L. B., Yang, Y., & Xu, Y. Q. (2021). Characterization of selenized polysaccharides from *Ribes nigrum* L. and its inhibitory effects on α-amylase and α-glucosidase. *Carbohydrate Polymers, 259*, Article 117729. https://doi.org/10.1016/j.carbpol.2021.117729

Zheng, Q. W., Jia, R. B., Luo, D. H., Lin, L. Z., Chen, C., & Zhao, M. M. (2022). The effect of extraction solution pH level on the physicochemical properties and α-glucosidase inhibitory potential of *Fucus vesiculosus* polysaccharide. *Lwt-Food Science and Technology, 169*, Article 114028. https://doi.org/10.1016/j.lwt.2022.114028

Zhou, D., Zhou, X., Shi, Q. L., Pan, J. B., Zhan, H. S., & Ge, F. H. (2022). High-pressure supercritical carbon dioxide extraction of Idesia polycarpa oil: Evaluation the influence of process parameters on the extraction yield and oil quality. *Industrial Crops and Products, 188*, Article 115586. https://doi.org/10.1016/j.indcrop.2022.115586

Zhou, Y. M., Duan, H. Y., Chen, J. S., Ma, S. J., Wang, M. L., & Zhou, X. L. (2023). The mechanism of in vitro non-enzymatic glycosylation inhibition by Tartary buckwheat's rutin and quercetin. *Food Chemistry, 406*, Article 134956. https://doi.org/10.1016/j.foodchem.2022.134956

Zhu, R. G., Zhang, X. Y., Wang, Y., Zhang, L. J., Zhao, J., Chen, G., … Ning, C. (2019). Characterization of polysaccharide fractions from fruit of *Actinidia arguta* and assessment of their antioxidant and antiglycated activities. *Carbohydrate Polymers, 210*, 73–84. https://doi.org/10.1016/j.carbpol.2019.01.037

Zor, T., & Seliger, Z. (1996). Linearization of the Bradford protein assay increases its sensitivity: Theoretical and experimental studies. *Analytical Biochemistry, 236*(2), 302–308. https://doi.org/10.1006/abio.1996.0171

Further reading

Chen, G. J., Li, C. F., Wang, S. S., Mei, X. F., Zhang, H. X., & Kan, J. Q. (2019). Characterization of physicochemical properties and antioxidant activity of polysaccharides from shoot residues of bamboo (*Chimonobambusa quadrangularis*): Effect of drying procedures. *Food Chemistry, 292*, 281–293. https://doi.org/10.1016/j.foodchem.2019.04.060

Li, M., Li, T., Hu, X. Y., Ren, G. Y., Zhang, H. A., Wang, Z. J., … Wu, J. R. (2021). Structural, rheological properties and antioxidant activities of polysaccharides from mulberry fruits (murus alba L.) based on different extraction techniques with superfine grinding pretreatment. *International Journal of Biological Macromolecules, 183*, 1774–1783. https://doi.org/10.1016/j.ijbiomac.2021.05.108

Liu, Y., Luo, M. L., Liu, F., Feng, X., Ibrahim, S. A., Cheng, L., & Huang, W. (2020). Effects of freeze drying and hot-air drying on the physicochemical properties and bioactivities of polysaccharides from *Lentinula edodes*. *International Journal of Biological Macromolecules, 145*, 476–483. https://doi.org/10.1016/j.ijbiomac.2019.12.222

Yang, M., Ren, W., Li, G., Yang, P., Chen, R., & He, H. (2022). The effect of structure and preparation method on the bioactivity of polysaccharides from plants and fungi. *Food & Function, 13*(24), 12541–12560. https://doi.org/10.1039/d2fo02029g

Yuan, Q., He, Y., Xiang, P. Y., Wang, S. P., Cao, Z. W., Gou, T., … Wu, D. T. (2020). Effects of simulated saliva-gastrointestinal digestion on the physicochemical properties and bioactivities of okra polysaccharides. *Carbohydrate Polymers, 238*, Article 116183. https://doi.org/10.1016/j.carbpol.2020.116183

Zheng, Q. W., Jia, R. B., Ou, Z. R., Li, Z. R., Zhao, M. M., Luo, D. H., & Lin, L. Z. (2022). Comparative study on the structural characterization and α-glucosidase inhibitory activity of polysaccharide fractions extracted from *Sargassum fusiforme* at different pH conditions. *International Journal of Biological Macromolecules, 194*, 602–610. https://doi.org/10.1016/j.ijbiomac.2021.11.103